Taurine is a Natural Host Cytoadhesion Inhibitor in Asymptomatic Malaria Cases

Authors: Gretchen Diffendall[1*], Perine Millot[2], Patty Chen[1], Balotin Fogang[4], Dominique Dorin-Semblat[2], Fanny Aprahamian[3], Sylvère Durand[3], Benoît Gamain[2], Antoine Claessens[4,5*] and Artur Scherf [1*]

Affiliations: [1]*Institut Pasteur, Biology of Host-Parasite Interactions Unit, INSERM U1201, CNRS EMR9195 ; Paris, France.*

[2]*Sorbonne Université, INSERM, CNRS, Centre d'Immunologie et des Maladies Infectieuses, CIMI F-75013 ; Paris, France.*

[3]*Metabolomic platform of Gustave Roussy, U1138/UMS AMMICa (US 23 INSERM / UMS 3655 CNRS); Paris, France*

[4]*LPHI, MIVEGEC, CNRS, INSERM, University of Montpellier, France*

[5]*Medical Research Council Unit The Gambia at the London School of Hygiene and Tropical Medicine, Banjul, The Gambia*

**Corresponding authors: artur.scherf@pasteur.fr, antoine.claessens@umontpellier.fr, gdiffendall@hsph.harvard.edu*

One Sentence Summary:

Metabolomics uncovers taurine as a natural host inhibitor of *Plasmodium falciparum* cytoadhesion in asymptomatic malaria carriers, offering new insights for disease control.

Abstract:

The prolonged dry season in malaria-endemic regions of sub-Saharan Africa can be divided into periods of high and low transmission. The majority of symptomatic malaria cases are restricted to the short high transmission period that follows the rainy season. Shortly after, persistent asymptomatic malaria cases are more prevalent throughout the prolonged low transmission period. It is still unclear whether host metabolic alterations play a role in asymptomatic infections during seasonal malaria. In this study, we analyzed the blood plasma metabolome (n=199) of individuals in The Gambia, West Africa, capturing data from both high

and low malaria transmission periods. Plasma samples from individuals (n=16) were collected monthly throughout the low transmission season, enabling a longitudinal analysis of metabolic alternations over six months. Our findings reveal that significant changes in host plasma metabolite composition are associated with seasonality and malaria pathogenicity. Notably, we observed elevated levels of taurine in asymptomatic malaria infections, especially during periods of low transmission. *In vitro*, this naturally occurring host molecule inhibits the cytoadhesion of malaria-infected red blood cells (iRBCs), which is key to malaria disease severity and mortality. Exogenous taurine can significantly reduce or reverse binding of iRBCs to the common adhesion receptor CD36 and the endothelial protein C receptor (EPCR), the later being associated with cerebral malaria. This study uncovers a mechanism by which elevated taurine plasma levels in asymptomatic infections could reduce cytoadhesion and lead to increased splenic clearance, thereby strengthening host resistance to symptomatic infections. In the absence of health strategies targeting dry season parasite reservoirs, our findings highlight taurine as a potential prophylactic or therapeutic agent to reduce symptomatic malaria in sub-Saharan Africa.

Main Text:

INTRODUCTION

Malaria, a mosquito-borne disease, remains a significant global health issue, causing nearly 600,000 deaths annually, with the majority occurring among children in sub-Saharan Africa [1]. Most fatalities are due to infection by *Plasmodium falciparum*, which produces adhesive proteins known as PfEMP1 on the surface of infected red blood cells (iRBCs) [2]. These proteins enable the parasite to bind to endothelial cells in various organs in a process called cytoadhesion, helping it to evade clearance by the spleen. The accumulation of parasites in organs is associated with symptomatic malaria, and when this occurs in the brain, it can lead to cerebral malaria, a more severe form of the disease [3]. Due to its central role in virulence, PfEMP1 is one of the most extensively studied surface protein families, consisting of 60 members per genome. By switching expression between these family members, iRBCs can exhibit different adhesive properties and antigenic variants, enabling them to evade the immune system and to sequester in different organs [4,5].

The extracellular domain of PfEMP1 proteins is comprised of 2-10 Duffy-binding-like (DBL) domains and cysteine-rich interdomain regions (CIDR) [6–9]. Individual domains commonly act

as specific receptor-binding regions of endothelial surface receptors [10]. Despite the significant sequence diversity among PfEMP1 family members, the N-terminal CIDRα domains retain a structural configuration that allows binding to either CD36 (CIDRα2-6) [11,12] or EPCR (CIDRα1) [10,13,14]. CD36 is predicted to be the most common adhesive phenotype in the PfEMP1 family, since approximately 84% of PfEMP1 proteins bind CD36 [10]. This scavenger receptor, commonly expressed on endothelial and innate immune cells, interacts with iRBCs from laboratory strains and field isolates. Apart from preventing splenic clearance, binding to CD36 expressed on dendritic cells may also inhibit the host innate immune response to infection [15,16]. A subset of 5-7 PfEMP1 members are predicted to bind to EPCR on brain endothelial cells [17,18] and has been associated with severe childhood malaria [13,19] and notably cerebral malaria [20,21].

Several studies have demonstrated that environmental sensing is a crucial aspect of the pathogen, modulating its proliferation, virulence gene expression, and developmental pathways [22–27]. In the context of environmental sensing, a phenomenon known as seasonal malaria in Sub-Saharan countries is of particular interest [28,29]. In these malaria-endemic regions, asymptomatic *P. falciparum* infections during periods of low transmission alternate with symptomatic infections during periods of high transmission. The influence of environmental changes on parasite virulence regulation and clinical manifestations remains a compelling area of investigation. Several epidemiological studies investigating factors that decrease symptomatic infections have been performed in Mali. The antibody response in asymptomatic individuals in Mali did not provide evidence that the immune response plays a major role in asymptomatic infections [29]. However, the same authors observed an extended blood circulation time of infected red blood cells (iRBCs) in asymptomatic individuals, suggesting that enhanced clearance by the spleen reduces parasite load and clinical symptoms. The factors contributing to this phenotype remain unknown [29–32].

Over the course of a year, The Gambia can be divided into periods of high transmission (late September through mid-December), when mosquitoes are more prevalent to transmit *P. falciparum* parasites to new human hosts, and periods of low transmission (late December through mid-September), when transmission is reduced (Fig. 1A) [33]. Both high and low transmission periods occur during the dry season (mid-September through mid-June) whereas the wet season is limited to late June through early September. After the high rain levels cease in September, symptomatic infections are limited to the high transmission months. A sizeable

fraction of infections remain chronic, resulting in asymptomatic infections being detected throughout the year, not limited to a specific period [34].

Although metabolomic analyses of human plasma from *P. falciparum*-infected individuals, have been conducted, most have focused on the effects of disease severity [35,35–39] rather than on seasonal variations in malaria. To our knowledge, only one recent study [32] has examined the impact of persistent asymptomatic infections on host plasma metabolites in Mali. However, its small sample size may have limited the ability to detect significant metabolic alterations.

In this study, we explored whether the dry season affects the host plasma environment of infected individuals, with a particular focus on identifying metabolites associated with disease severity and seasonal impact on asymptomatic infections. Metabolite profiling was performed on human plasma samples (n = 199) collected from individuals in The Gambia, including those infected with *P. falciparum*—both symptomatic and asymptomatic—as well as non-infected volunteers, as part of a previously conducted two-part study[33,40].

Our results reveal significant changes in metabolite levels associated with malaria severity—comparing symptomatic and asymptomatic infections during the high transmission season—as well as with seasonality, by comparing asymptomatic infections across high and low transmission periods. Notably, one of the most highly elevated metabolites in asymptomatic infections, consistently increased in asymptomatic infections, was taurine, an amino sulfonic acid. While taurine is synthesized in the liver from methionine and cysteine, it is not a component of proteins but plays a role in various physiological host functions [reviewed in [41]]. Although taurine showed no effect on iRBCs development of cultured parasites, it strongly inhibited iRBCs adhesion to CD36 and EPCR receptors as well as by a human cell line expressing CD36 at concentrations observed in dry season-infected individuals. Additionally, taurine was able to reverse iRBCs binding to these receptors. The identification of a natural host molecule that inhibits iRBC binding to CD36 and EPCR offers a novel therapeutic and prophylactic strategy to target symptomatic malaria and reduce dry-season reservoirs.

RESULTS

Study design and metabolomics analysis

131 To investigate host metabolic changes during malaria infection, we analyzed a total of 199
132 plasma samples collected from individuals living in neighboring villages in The Gambia (Fig.
133 1A) as part of a previously published longitudinal study [33,40]. The cohort design included two
134 complementary arms: (1) During the high transmission season (October–November), active
135 case detection yielded 46 blood samples from asymptomatic *P. falciparum* carriers, while
136 individuals presenting at local health posts yielded 38 samples from symptomatic malaria case.
137 (2) During the low transmission season (December–May), a subset of 16 asymptomatic
138 individuals with persistent *P. falciparum* infections was followed monthly for up to 6 months.
139 Also included were 9 unique asymptomatic individuals that had samples taken in December.
140 Additionally, 11 non-infected individuals were sampled between December to February.
141
142 As expected, parasite loads were significantly higher in symptomatic individuals (Fig. S1A).
143 Although participants were not age-matched across groups, the overall age distribution was
144 representative of the local population (median age: 19 years, Fig. S1B–C, [33]). Metabolomics
145 was performed on a total 199 plasma samples using gas chromatography coupled to triple
146 quadrupole mass spectrometry (GC–QqQ/MS), targeting a broad panel of compounds. After
147 quality filtering, 78 metabolites were retained for analysis (Fig. 1B), spanning diverse chemical
148 classes including amino acids, fatty acids, and carbohydrates (Fig. 1C). These metabolites play
149 a role in various metabolic pathways, determined by pathway enrichment analysis (Fig. 1D,
150 SM3). Initial Principal component analysis (PCA) revealed clustering of samples according to
151 infection status and season (Fig. 1E).
152

153 **Metabolites associated with seasonality**

154 We assessed the influence of seasonality on host metabolic responses by comparing
155 asymptomatic infections from the peak transmission period (October) with those from the end
156 of the dry season (May), when rainfall has been absent for over seven months and malaria
157 transmission is nearly absent. Seventeen metabolites differed significantly between these
158 timepoints (Wilcoxon test, adjusted for multiple comparisons with Benjamini-Hochberg
159 correction , Fig 2A, SM5). The most significant increase in May was observed for taurine
160 (adjusted p-value < 0.00379). These results indicate that the dry season influences host plasma
161 metabolites, possibly through changes in diet or microbiota composition.

162 **Metabolites associated with symptomatic malaria**

163 To identify metabolic signatures associated with malaria symptoms, we compared 38
164 individuals with symptomatic infections to 46 asymptomatic infections collected during the
165 same high-transmission months (October–November). We used a mixed-effects model with
166 month as a random effect and metabolites as fixed effects. After multiple testing correction, 27
167 metabolites were significantly associated with clinical status, with 16 elevated and 11 reduced
168 in symptomatic individuals (Fig. 2 B&C, SM5). Among the metabolites elevated in
169 symptomatic individuals were: (1) 2-oxoglutaric acid (more commonly known as alpha-
170 ketoglutarate, a TCA cycle intermediate, previously identified as a biomarker of *P. falciparum*
171 infection [36]. (2) lactic acid, consistently reported as elevated in symptomatic malaria. (2)
172 Palmitoleic acid, a monounsaturated fatty acid that may accumulate during *P. falciparum*
173 infection [42]. (4) 3-hydroxybutyric acid, a fatty acid derivative that accumulates during parasite-
174 induced acidosis [43] and has been shown to inhibit *P. falciparum* growth *in vitro* [44].
175 Conversely, multiple amino acids (aspargine, citrulline, aspartic acid) and other metabolites
176 (guanosine , maltose;trehalose) were reduced in symptomatic infections. Taurine levels were
177 also lower, though less markedly (Odds Ratio 0.553, adjusted p-value = 0.0503). These
178 findings reveal a distinct metabolic host signature associated with symptomatic malaria,
179 highlighting disruptions in energy metabolism and fatty acid pathways during acute *P.*
180 *falciparum* infection.

181 **Metabolite dynamics during chronic asymptomatic infection in the dry season**

182 We took advantage of the longitudinal monthly sampling from 16 individuals with persistent
183 asymptomatic infections over the low transmission season (December to May) to examine
184 temporal changes in plasma metabolites. Using a mixed-effects model with non-infected
185 individuals as controls, we identified nine metabolites—including several amino acids and
186 taurine—that consistently increased over time, particularly from March onward (Fig S2A,
187 SM5). In contrast, allantoin and glycerol-3-phophate showed the opposite trend, with higher
188 levels early in the low transmission season and lower levels later (Fig. S2A, SM5). These
189 patterns likely reflect a combination of dietary shifts and host physiological adaptations. For
190 instance, allantoin, an oxidative product of urate, is a marker of oxidative stress; valine,
191 isoleucine and methionine are diet-derived; taurine can be either diet-derived or endogenously
192 synthesized, and plays a protective role against oxidative stress [45].

193

194 Finally, we used a mixed-effects model to assess whether the host metabolome differentiates
195 asymptomatic carriers during the low transmission season from uninfected individuals. Only
196 two metabolites, capirc acid and aminovaleric acid, were associated with infection status,
197 indicating a weak effect of an asymptomatic infection on the overall metabolome (SM5).
198 Nevertheless, the dynamic shift in specific plasma metabolites across the low transmission
199 season likely reflect dietary changes and host physiological adaptations, including responses
200 to oxidative stress.

201 This dataset motivated us to identify metabolites potentially involved in modulating *P.*
202 *falciparum* persistence and virulence. We prioritized metabolites meeting three progressively
203 less stringent criteria: (1) higher levels in May compared to the peak transmission season
204 (October), (2) a consistent increase across the low transmission season, (3) lower levels in
205 asymptomatic than in symptomatic cases. Taurine emerged as the strongest candidate, fulfilling
206 all three conditions (Fig. S2B). These findings led us to further investigate the functional role
207 of taurine in malaria pathogenesis, a direction supported by a recent study showing that taurine
208 supplementation in a *P. berghei* mouse model conferred host benefits through immune
209 modulation [46].

210 **Taurine inhibits ability of iRBCs to cytoadhere to CD36 and EPCR**

211 Given the key role of iRBC adhesion in malaria pathogenesis, our goal was to identify
212 candidate metabolites significantly elevated in asymptomatic infections during the low
213 transmission period that may influence *P. falciparum* sequestration to endothelial receptors.
214 Additionally to taurine, threonic acid, a breakdown product of ascorbic acid, was selected due
215 to previous findings that ascorbic acid significantly inhibits *P. falciparum* growth; however, its
216 potential effect on iRBC cytoadhesion has not yet been studied [47]. We next investigated
217 whether taurine and threonic acid could reduce iRBC cytoadhesion *in vitro*. To establish
218 physiologically relevant high and low taurine concentrations for the cultures, we measured the
219 absolute taurine quantity in plasma samples exhibiting the highest and lowest values from our
220 mass spectrometry analysis. The lowest values corresponded to taurine concentrations of
221 [0.009mM], [0.026mM], and [0.032mM] while the highest values corresponded to [0.113mM],
222 [0.175mM], and [0.176mM]. These taurine concentrations aligned with levels reported in
223 human plasma [48] and confirmed the mass spectrometry results. Due to the absence of an assay
224 kit for threonic acid, a reported physiological concentration of 0.27 mM [49] was used for all
225 analyses. Growth curve analysis of wild-type *P. falciparum* cultures supplemented with or

226 without various taurine concentrations, or threonic acid [0.27mM] (Fig. S3A) revealed no
227 effect of taurine nor threonic acid on growth over the course of five days. These data are
228 consistent with what was observed in another study [50] at even higher concentrations of taurine.
229 Physiological taurine levels ranging from 0.64 to 0.93 mM have been observed in clinical
230 volunteer studies following oral administration of 4 g of taurine [51].
231
232 To determine if adhesion of iRBCs is affected by taurine or threonic acid, we performed
233 adhesion assays with RBCs infected with late-stage wild-type 3D7 parasites grown in media
234 supplemented with a range of taurine concentrations for up to 40 hours (Fig. 3A, S3B). The
235 lowest taurine concentration of [0.02mM] already significantly decreased adhesion of iRBCs
236 to CD36 ($p < 0.0001$) by up to 60% (Fig. 3A). With even higher taurine concentrations, binding
237 was drastically decreased by > 97% (Fig. 3A, B). Thus, physiological levels of plasma taurine
238 found in asymptomatic individuals almost completely blocks binding of iRBCs to recombinant
239 CD36 receptor *in vitro*. Threonic acid, at physiological levels of [0.27mM] [49], had no
240 significant effect on adhesion of iRBCs to CD36 (Fig. S3C). As metabolomic MS analysis
241 revealed no significant differences in methionine levels between conditions (SM4), a
242 physiological concentration of 0.04 mM was used as a control, which also had no significant
243 effect on adhesion (Fig. 3A) [52]. Incubation of iRBCs with [0.16mM] of taurine for one hour
244 prior to the adhesion assays was sufficient to decrease cytoadhesion by > 97% (Fig. 3A),
245 suggesting that taurine influences iRBC adhesion through direct interaction with the iRBC
246 surface, rather than by altering parasite transcription or protein expression on the surface of
247 iRBC.
248
249 The surface PfEMP1 domains that bind to CD36 and EPCR are associated with a single CIDR
250 domain [53]. We next set out to determine if taurine affects iRBC binding to the endothelial cell
251 protein C receptor (EPCR), which is important in cerebral malaria [13]. We used a parasite strain
252 (FCR3) that predominantly express the Itvar19 PfEMP1 previously found to bind to EPCR [54].
253 After a one-hour incubation with [0.16mM] or [0.64mM] taurine, we observed a significant
254 decrease in adhesion of FCR3 iRBCs to recombinant EPCR of almost 50% and >70%,
255 respectively (Fig. 3C). This parasite line, which also expresses a distinct PfEMP1 member was
256 additionally used for adhesion assays with CD36 (Fig. S3D). Taurine supplementation
257 similarly reduced receptor binding across strains, indicating that taurine inhibitory effect is not
258 strain specific and is effective despite differences in *var* gene family repertoires.
259

260 In contrast to adhesion of infected red blood cells to CD36 and EPCR, which involves diverse
261 PfEMP1 variants containing CIDR domains, adhesion to placental chondroitin sulfate A (CSA)
262 is mediated by a unique PfEMP1 encoded by the *var2CSA* gene, which comprises multiple
263 DBL domains but lacks a CIDR domain [53]. We performed iRBC adhesion assays with the
264 NF54 parasite strain that expresses VAR2CSA [55] in the presence or not of [0.64mM] taurine
265 (Fig. S3E). A small but significant decrease in iRBC binding was observed ($p = 0.0288$).
266 Finally we assessed the capacity of malaria naïve human serum to inhibit iRBC binding to
267 CD36. Human serum caused a slight reduction in our iRBC binding assay (Fig. S3F),
268 comparable to the effect of 0.02 mM taurine supplementation (Fig. 3B), likely due to the taurine
269 content in the serum used for parasite culture, which reached up to 0.02 mM. Our findings
270 show that physiological taurine levels inhibit iRBC adhesion to CD36 and EPCR, pointing to
271 a novel host-mediated mechanism contributing to reduced *P. falciparum* virulence in
272 asymptomatic infections.
273
274 **Taurine reverses adhesion of iRBCs to CD36 and EPCR**
275 To assess its therapeutic potential, we set out to determine if taurine could reverse, rather than
276 merely prevent, iRBC binding to CD36 (Fig. 4A) and EPCR (Fig. 4B), using the same strains
277 from (Fig. 3B, D). When iRBCs already adhering to CD36 or EPCR were incubated without
278 or with [0.64mM] taurine for 45 minutes, adhesion decreased by over 77% ($p < 0.0001$) to
279 CD36 and nearly 30% ($p = 0.0017$) to EPCR (Fig. 4A, B). These demonstrate that taurine can
280 disrupt existing interactions of iRBCs with endothelial receptors.
281
282 To explore the mechanisms by which taurine inhibits and reverses iRBC binding to endothelial
283 receptors, we examined PfEMP1 expression. Since a one-hour taurine incubation was sufficient
284 to nearly abolish completely iRBC adhesion, it is unlikely that transcriptional changes could
285 account for such rapid effects on protein expression. Indeed, FACS analysis of FCR3 Itvar19
286 iRBCs supplemented with taurine showed no significant changes in surface PfEMP1 protein
287 levels (Fig. S4A, S4B, C). We additionally tested whether taurine interacts directly with CD36
288 to prevent iRBC binding. iRBC adhesion assays were performed with CD36 receptors that
289 were pre-treated with or without [0.16mM] taurine and no significant difference in adhesion of
290 iRBCs was observed between the two conditions (Fig. S4D). The observed rapid action of
291 taurine suggests it may directly target the iRBC surface, inducing conformational changes in
292 parasite adhesins and thereby altering binding properties.
293

294 **Taurine reduces binding of iRBCs to CD36 on human C32 melanoma cells**

295 To investigate taurine inhibition in a cellular context, we employed the human C32 amelanotic
296 melanoma cell line, which has been used extensively in previous *P. falciparum* CD36 adhesion
297 studies [56]. This cell line shares adhesion receptors with human endothelial cells, and the
298 mechanisms of binding are comparable, making it a suitable surrogate for endothelial cells in
299 adhesion assays [57,58]. Parasitized erythrocytes primarily adhere to these melanoma cells via the
300 glycoprotein CD36, which is also widely expressed on vascular endothelium [59]. In three
301 biological replicates we observed > 60% inhibition of FCR3 strain adhesion to C32 at taurine
302 concentration of 0.93 mM. This inhibition was dose-dependent (Fig. 4C, D). Similar C32
303 inhibition results were obtained using a genetically distinct strain (3D7) (Fig. S4E, F). Taurine
304 inhibits iRBC adhesion at the cellular level, albeit at higher concentrations than with
305 recombinant receptors. Its effectiveness in reducing iRBC binding by multiple methods,
306 highlights its potential as a natural supplement to lessen disease severity in endemic areas.
307

308 **DISCUSSION**

309 The mechanisms by which *P. falciparum* persists through the rainy season without causing
310 symptoms remain unclear. In this study, we investigated if environmental factors contribute to
311 asymptomatic and persistent *P. falciparum* infections during the dry season in sub-Saharan
312 Africa. To do so, we conducted a metabolomics analysis on plasma samples collected from
313 infected and non-infected individuals in The Gambia, West Africa, from both high and low
314 transmission times during the dry season (Fig. 1). Of the statistically validated metabolites
315 identified (n=78), forty-three showed distinct profiles in the cohort (Fig. 2C). We identified
316 metabolites that are dependent on disease severity or seasonality. Metabolites associated with
317 severity include fatty acids, which have been shown to increase in *P. falciparum* infections, as
318 well as a previously identified biomarker involved in the TCA cycle [36]. Metabolites linked to
319 seasonality include those potentially derived from the diet, as well as metabolites produced
320 endogenously by the host to combat oxidative stress.
321

322 Since the development and proliferation of *P. falciparum* rely on nutrient uptake from the host
323 serum [60], the observed changes in the host metabolome may directly affect the parasite.
324 However, it remains unclear whether the altered metabolite levels—either elevated or
325 reduced—are taken up by iRBCs and subsequently influence parasite development. Of note, a
326 recent report suggests that external lactate levels, a major cause of parasite-induced acidosis,

327 may serve as metabolic sensors in *P. falciparum* iRBCs [61]. An increase in environmental lactate
328 was linked to elevated levels of epigenetic regulators, *sirtuins* [62], and histone lysine lactylation
329 [61] in the parasite. In our study, lactate levels were significantly lower in asymptomatic
330 infections compared to those with symptomatic infections during the high transmission period.
331 Another major contributor to parasite-induced acidosis, 3-hydroxybutyric acid, was found
332 significantly increased in our symptomatic high transmission infections [43].
333
334 One of the most striking metabolic changes observed was in taurine levels, which were as low
335 as 0.02 mM during periods of high transmission and rose to 0.16 mM by the end of the low
336 transmission season in infected individuals. For comparison, oral administration of taurine (4
337 g) in eight healthy volunteers increased plasma levels from 0.03–0.06 mM to peak
338 concentrations of 0.53–0.93 mM for several hours after taurine administration [51]. The cause of
339 elevated taurine levels in individuals with asymptomatic infections remains unclear. Although
340 the human liver synthesizes taurine, dietary sources such as meat, fish, poultry, and dairy also
341 contribute to plasma levels. In rural Gambia, diets mainly consist of rice, wheat-flour bread,
342 and groundnuts, with seasonal availability of leafy vegetables, millet, and dried fish. Since
343 there's no evidence of increased protein intake during the dry season in this cohort, we
344 hypothesize that elevated plasma taurine levels are due to increased endogenous bile secretion.
345 Notably, persistent high host-derived taurine levels have been reported for extended periods
346 following the resolution of enteric infections in mice [63]. It would be important to investigate
347 whether changes in the gut microbiome play a role in stimulating increased bile taurine
348 production in this cohort.
349
350 Although taurine treatment did not affect parasite growth (Fig. S3A), it strongly inhibited the
351 binding of iRBCs to recombinant receptor CD36 (Fig. 3A) and to a lesser degree to the brain
352 endothelial receptor EPCR (Fig. 3C). Conversely, taurine had a very mild effect on adhesion
353 of RBCs infected with parasites expressing an atypical PfEMP1 family member (VAR2CSA)
354 that has no CIDRα domain (Fig. S3E). Importantly, we show that taurine inhibits iRBC
355 adhesion to the human C32 melanoma cell line, a common endothelial surrogate in *P.*
356 *falciparum* CD36 adhesion assays (Fig. 4C).
357
358 Since taurine preincubation with CD36 did not affect iRBC binding (Fig. S4D), it likely
359 disrupts adhesion by targeting PfEMP1–receptor interactions, possibly at the CIDR-binding
360 domain. Multiple findings support this hypothesis. Taurine pretreatment of adhesive iRBCs for

361 one hour significantly reduced CD36 binding (Fig. 3A) without affecting PfEMP1 surface
362 expression (Fig. S4A), suggesting the effect is not due to altered protein trafficking. Its
363 selective inhibition of CD36 and EPCR binding points to disruption of specific PfEMP1
364 interactions rather than general membrane effects. Notably, taurine reversed adhesion to CD36
365 by over 77% and to EPCR by over 29% (Fig. 4A, B). For CD36, binding inhibition was
366 consistent across CD36-binding strains (3D7 and FCR3), despite sequence variability in the
367 CIDRα domain [11].
368
369 A study conducted in Mali[29] provided evidence that increased circulation time of infected red
370 blood cells (iRBCs) is associated with asymptomatic infections during the dry season, although
371 the underlying mechanism was not elucidated. Our findings from The Gambia offer
372 mechanistic support for these observations, suggesting that elevated plasma taurine levels in
373 persistent asymptomatic infections may reduce or reverse iRBC binding, thereby promoting
374 the circulation of mature parasite forms and their clearance by the spleen. In a recent small-
375 scale plasma metabolomics study involving 35 samples from 20 individuals with symptomatic
376 and asymptomatic infections in Mali, taurine levels were not reported [32]. Further studies are
377 needed to explore whether elevated plasma taurine levels are a consistent feature of
378 asymptomatic *P. falciparum* infections during the dry season across sub-Saharan Africa. It
379 cannot be excluded that, in addition to taurine, other metabolites associated with plasma
380 alterations in asymptomatic malaria contribute to asymptomatic malaria by influencing the
381 iRBC proliferation or by increasing their susceptibility to immune-mediated clearance.
382
383 Other host receptors such as ICAM-1 have been linked to severe malaria and aggregation of
384 iRBCs and uninfected RBCs (known as rosettes) [reviewed in [2]]. Both adhesion phenotypes
385 are significantly rarer than CD36 adhesion and it remains to be shown if these phenotypes play
386 an important role in symptomatic infections during seasonal malaria.

387 Binding of *P. falciparum* iRBCs to human receptors is central to the development of
388 symptomatic and severe malaria. Yet, no adjunctive therapies or broad-spectrum vaccines
389 currently target CD36-binding parasites, and efforts to block EPCR-binding variants
390 implicated in severe and cerebral malaria remain ongoing [64]. Clinically, taurine is already used
391 as a dietary supplement with documented benefits for conditions like hypertension and
392 hypercholesterolemia [reviewed in [65]]. Our identification of taurine, a natural host molecule,
393 as an effective inhibitor of iRBC binding to both CD36 and EPCR reveals a novel public health

394 strategy to reduce or eliminate dry-season reservoirs and prevent symptomatic malaria at the
395 start of the transmission season.

396 **MATERIALS AND METHODS**

397 **Study individuals and ethical approval**

398 Study design and sample collection was alredy reported in [33,34,40]. The first part of the study
399 was a cross-sectional study implemented in October and November 2016 to estimate the
400 prevalence of *P. falciparum* infections in four neighboring villages (Madina Samako: K,
401 Njayel: J, Sendebu: P, and Karandaba: N) within a 5km radius in Upper River Region (URR),
402 eastern Gambia. *P. falciparum* asymptomatic infections were detected by varATS qPCR and
403 individuals were invited to provide a venous blood sample before receiving anti-malarial
404 treatment. Symptomatic cases presented themselves at the local health facility with fever.
405 Malaria cases were defined as anxially temperature >37.5C, positive RDT and later
406 confirmation of *P. falciparum* infection by varATS qPCR. For the second part of the study, in
407 December 2016, asymptomatic *P. falciparum* carriers were recruited for a longitudinal cohort
408 with monthly samplings until May 2017, or until the infection naturally cleared [Ref
409 Collins2022].
410
411 The high transmission season months include October and November and the low transmission
412 season months include late December, January, February, March, April, and May. The months
413 pertaining to the two transmission periods was directly determined by the reports of
414 symptomatic malaria infections for that specific year for all villages used in the study [33]. For
415 additional information about each sample, see (SM1).
416
417 The study protocol was reviewed and approved by the Gambia Government/MRC Joint Ethics
418 Committee (SCC 1476, SCC 1318, L2015.50) and by the London School of Hygiene &
419 Tropical Medicine ethics committee (Ref 10982). The field studies were also approved by local
420 administrative representatives, the village chiefs. Written informed consent was obtained from
421 participants over 18 years of age and from parents/guardians for participants under 18 years.
422 Written assent was obtained from all individuals aged 12–17 years.
423

424 **Human plasma sample collection**

425 From *P. falciparum* positive individuals (by varATS qPCR), 5 to 8mL venous blood was
426 collected in a EDTA vacutainer. Collected venous blood samples were immediately separated
427 in plasma, PBMCs and red blood cells, by centrifugation on a layer of Lymphoprep™
428 according to manufacturer's instructions. Plasma was directly stored at -80 degrees Celsius
429 and never thawed until use in this study.

430

431 **Metabolomics of human plasma sample preparation and widely targeted detection by**
432 **GC-MS**

433 50 µl of collected plasma were mixed with 500 µl of ice-cold extraction mixture
434 (methanol/water, 9/1, -20°C, with labelled internal standard). To facilitate endogenous
435 metabolites extraction, samples were then completely homogenized (vortexed 5 minutes at
436 2500 rpm) and then centrifuged (15 min at 10000 g, 4°C). 150 µl of supernatants were collected
437 to be analyzed by gas chromatography coupled with mass spectrometer (GC/MS) [66].

438

439 Widely targeted analysis by GC-MS/MS was performed on a 7890A gas chromatography
440 (Agilent Technologies) coupled with Triple Quadrupole 7000C (Agilent Technologies) and
441 was previously described in [67]. All targeted treated data were merged and cleaned with a
442 dedicated R (version 4.0) package (@Github/Kroemerlab/GRMeta).

443

444 **Plasma taurine concentration assay**

445 Plasma taurine levels were determined using a commercial taurine assay kit (Cell Biolabs
446 MET-5071). Complete information on tested individual samples can be found in (SM1). The
447 protocol was followed as described in the kit and read on a Synergy 2 microplate reader for
448 spectrophotometric reading.

449

450 **Parasite culture and synchronization**

451 Asexual blood stage *P. falciparum* parasites were cultured as previously described in [68].
452 Parasites were cultured in human RBCs (obtained from the Etablissement Français du Sang
453 with approval number HS 2019-24803) in RPMI-1640 culture medium (Thermo Fisher 11875)
454 supplemented with 10% v/v Albumax I (Thermo Fisher 11020), hypoxanthine (0.1 mM final
455 concentration, C.C.Pro Z-41-M) and 10 mg gentamicin (Sigma G1397) at 4% hematocrit and
456 under 5% O_2, 3% CO_2 at 37 °C. Static parasite development was monitored by Giemsa staining.
457 Parasites were synchronized by sorbitol (5%, Sigma S6021) lysis at ring stage, plasmagel

458 (Plasmion, Fresenius Kabi) enrichment of late stages 24 hours later, and an additional sorbitol
459 lysis 3 hours after plasmagel enrichment. The 0-hour time point was considered to be 1.5 hours
460 after plasmagel enrichment.
461
462 **Parasite growth assay**
463 Parasite growth was measured as described previously [69]. Wild type 3D7 parasites were tightly
464 synchronized and diluted to 0.2% parasitemia (5% hematocrit) at the ring stage using the blood
465 of three different donors separately (n=3). Each culture was split into control and parasites
466 supplemented with [0.16mM] taurine. The growth curve was performed with three technical
467 replicates per condition per blood. Parasitemia was measured every 24 hours by counting ten
468 randomly selected different fields on Giemsa-stained slides each day for a total of five days.
469
470 **Static iRBC adhesion binding assays**
471 3D7-CD36 Binding Assay: Mature-stage iRBCs (3D7 strain) were used for iRBC adhesion
472 assays as previously described [70]. Taurine was supplemented at increasing concentrations
473 (0.02, 0.04, 0.08, and 0.16 mM) from a 200 mM stock to cultured parasites. Methionine (0.04
474 mM) was added post-synchronization. For short-term treatments, 0.16 mM taurine or 0.27 mM
475 threonic acid was added one hour prior to the assay. All compounds were removed before
476 adhesion assays via plasmagel enrichment of mature iRBCs. Recombinant receptors diluted in
477 Dulbecco's phosphate-buffered saline (DPBS, Thermo Fisher 14190) (10 µg/mL target CD36
478 or negative control 1% BSA) were spotted on labeled petri dishes overnight at 4°C in duplicate.
479 Dishes were blocked for 30 minutes at 37°C with 1% BSA/DPBS while parasitemia was
480 determined after trophozoite and young schizont iRBCs were isolated by plasmagel (Plasmion,
481 Fresenius Kabi) enrichment. Adjusted amounts of iRBCs were resuspended in DPBS for a
482 concentration of 2.2×10^8 iRBCs/mL. iRBCs/DPBS were added to each petri dish and
483 incubated for one hour at 37°C. Unbound cells were removed, and the dishes were washed five
484 times with DPBS by carefully tilting from side to side. Adherent iRBCs were counted in
485 duplicate spots using 40x lens with a Nikon ECLIPSE TE200 in seven randomly selected fields
486 (each with 0.2 mm^2) using ImageJ2 (version 2.14.0/1.54i). A total of three biological replicates
487 were performed in duplicate and the results were expressed as the percentage of bound iRBCs
488 compared to the control per 0.2 mm^2 of target receptor monolayer.
489
490 FCR3-*var19*-EPCR and FCR3-CD36 binding assay: For EPCR binding, the protocol listed
491 above was followed with the following changes: Recombinant receptors were diluted in in

492 DPBS (50 µg/mL EPCR, 50 µg/mL CD36 or negative control 1% BSA) were spotted on
493 labeled petri dishes overnight at 4°C in duplicate. Late stage iRBCs from FCR3 *var19*-
494 expressing parasites [54] were purified by VARIOMACS (Miltenyi Biotec France) and counted.
495 The iRBC pellet was split into control and addition of taurine [0.64mM] for one hour in RPMI-
496 1640 culture medium (Thermo Fisher 11875) supplemented with 10% v/v Albumax I (Thermo
497 Fisher 11020), hypoxanthine (0.1 mM final concentration, C.C.Pro Z-41-M) and 10 mg
498 gentamicin (Sigma G1397) at 4% hematocrit and under 5% O_2, 3% CO_2 at 37 °C. The spots
499 were washed twice with DPBS and blocked for 30 minutes at room temperature with 1%
500 BSA/DPBS, 3.75 x 10^6 parasites/mL diluted in 10uL DPBS were added to each spot and
501 incubated for one hour at room temperature. Plates were gently washed with 25mL DPBS on
502 an orbital shaker for 2 minutes and repeated four times before visualization and imaging using
503 EVOS 5000. Adherent iRBCs were counted in duplicate spots using 20x lens with a Nikon
504 ECLIPSE TE200 in seven randomly selected fields (each with 0.3 mm^2).
505
506 NF54-*var2CSA*-CSA binding assay: For CSA binding, the protocol listed above (for 3D7-
507 CD36 binding) was followed for control and supplementation of [0.64mM] Taurine using
508 CSA-panned NF54 parasites [55,71].
509
510 Evaluation of taurine's ability to reverse iRBC binding to CD36 and EPCR: A two-step
511 protocol was used to evaluate the reversal of binding of 3D7 and FCR3-*var19*-expressing
512 parasites to CD36 or EPCR. In Step 1, binding was conducted as previously described for 3D7
513 to CD36 and FCR3-*var19* to EPCR. In Step 2, DPBS or [0.64mM] taurine + DPBS was added
514 for 45 minutes, followed by DPBS washes. Adherent iRBCs were counted in duplicate spots
515 using a 10x objective lens to count and assess the percent reduction in bound iRBCs after
516 taurine incubation compared to the control.
517
518 Taurine-CD36 incubation prior to iRBC adhesion assay: For CD36-Taurine binding, the
519 protocol was followed the same as listed above (for 3D7-CD36 binding) for mature stage
520 iRBCs from 3D7 parasites with the following changes: Control and supplementation of
521 [0.16mM] taurine was added during blocking stage with 1% BSA/DPBS.
522
523 Human serum- and human serum+taurine-CD36 binding assay: For human serum-CD36
524 binding and human serum + taurine-CD36 binding, the protocol was followed the same as
525 listed above (for 3D7-CD36 binding) for mature stage iRBCs from 3D7 parasites with the

526 following changes: 10% human serum without and with supplementation of [0.64mM] taurine
527 from three different donors (n=3) was added for one hour prior to the assay.
528
529 **C32 melanoma cell binding assay**
530 C32 melanoma binding assays were performed as previously described [72]. To prepare iRBCs
531 for the cellular inhibition assay, mature-stage iRBCs (3D7 or FCR3) were prepared as for the
532 receptor binding assays above. Plasma gel-enriched FCR3 iRBCs were overlaid onto confluent
533 C32 cell monolayers in 6-well plastic dishes for 45 minutes in binding medium. After a 1-hour
534 incubation, unbound iRBCs were removed by gentle washes with RPMI medium adjusted to
535 pH 6.8 until only adhering parasites were observed. For each taurine concentration, ten
536 independent 1 mm^2 microscopic fields were counted across three biological replicates. iRBC
537 adhesion was quantified by counting bound iRBC per mm^2 of confluent C32 cells in 10 random
538 fields. Representative micrographs and raw data are provided in the supplementary materials
539 (Fig. 4D, S4D, SM6).
540
541 **Flow cytometry assessment of *var19* surface expression**
542 Control and supplementation of [0.64mM] taurine in FCR3 *var19*-expressing parasites iRBCs
543 at mid/late trophozoites stages were resuspended in DPBS 1% BSA after VARIOMACS
544 purification and counted. For each assay, 3×10^5 iRBCs were washed in DPBS and incubated
545 with 50µl of purified rabbit anti-*var19* antibodies [54] diluted 1:100 in PBS 1% BSA for 1-hour
546 at room temperature. iRBCs were washed twice with DPBS and resuspended in 100µl of PE
547 conjugated goat anti-rabbit antibody diluted 1: 100 in DPBS for 30 min at RT. iRBCs were
548 washed twice in DPBS 1% BSA and resuspended in paraformaldehyde 4% in DPBS and kept
549 at 4°C overnight in darkness. Cells were washed twice with DPBS and analyzed by flow
550 cytometry using a BD LSR Fortessa flow cytometer. The results were analyzed using the
551 FlowJo 10.0 software. Parasite nuclei were stained by TO-PRO-3 (1:10000 dilution). The
552 results are expressed as the percentage of *var19* surface expression. A total of three biological
553 replicates (n=3) were performed.
554
555 **Statistical analysis**
556 For metabolomics MS analysis, GRmeta (https://github.com/kroemerlab/GRMeta) was used
557 for the data shape QC correction (based on global pool for normalization between 3 total
558 batches).
559

Fold change (FC) was determined when comparing each condition of each month to all other conditions in each month using the following code:

```
#Fold Change averages
mm = mergedata$Data$AreaCorrLog2Cen2
mm = cbind(as.data.frame(mergedata$Grp2),mm)
mm = apply(mm[,-1], 2, function(x) tapply(x, mm$`mergedata$Grp2`, mean)) %>% t()

FC = combn(1:ncol(mm),2,function(x) mm[,x[2]] - mm[,x[1]])
```

p values were determined when comparing each condition of each month to all other conditions in each month using Kruskall wallis with BH adjustment with the following code:

```
KruskalWallis$data[[mergedata$Annot$MetName[i]]]=as.data.frame(dunn.test(mergedata$
Data$AreaCorrLog2Cen2[,i],mergedata$Grp2, method="BH", kw=TRUE,
label=TRUE,wrap=FALSE, table=TRUE, list=FALSE, rmc=FALSE, alpha=0.05,
altp=FALSE)$P.adjusted)
```

Metabolite enrichment and pathway analyses was performed using the Over Representation and Quantitative Enrichment tools on the MetaboAnalyst 6.0 server (https://www.metaboanalyst.ca/), integrated with the KEGG database (https://www.genome.jp/kegg/). Input data included a list of compound names (KEGG and HMDB IDs) for metabolites passing GC-MS quality control, categorized by their specific class. Pathway-based analysis was performed with at least two entries in the metabolite set library, which includes 80 metabolite sets based on KEGG human metabolic pathways (Dec 2023). Results were visualized as dot plots displaying key information on enrichment ratios, p-values, and log2 values for the respective metabolite sets.

To identify metabolites associated with infection status while accounting for temporal and repeated-measures dependencies, we employed generalized linear mixed-effects models (GLMMs) with a binomial logit link. For symptomatic malaria (S vs AS), the model included the scaled metabolite level as a fixed effect and sample month (October, November) as a random intercept. For asymptomatic infection (AS vs NI), the model included the metabolite level as a fixed effect, with sample month (December, January, February) and individual included as random intercepts. For chronic asymptomatic (AS) infections across the dry season,

593 the model was extended to test for temporal effect modification. It included the fixed effects of
594 the metabolite level, time (month, from December to May), and their interaction term, with a
595 random intercept for individual.
596
597 All other statistical analyses were performed using R version 4.3.2 and GraphPad Prism version
598 9.1.0 (216) for Mac. To test for a normal distribution of the data, the Shapiro-Wilk normality
599 test was used. To test for significance between two groups, a two-sided independent-samples t
600 test was used.
601
602 **Supplementary Materials:**
603 Fig. S1 to S4
604 SM1 Information on samples from volunteers (excel file)
605 SM2 Metabolite alternative names (excel file)
606 SM3 Metabolomics MS raw data (excel file)
607 SM4 Pathway Enrichment Analysis (excel file)
608 SM5 Fold Change, p-values, and results from additional analyses to determine significantly
609 increased or decreased metabolites depending on severity and seasonality (excel file)
610 SM6 iRBC adhesion counting raw data (excel file)
611
612 **Fig. 1: Blood Plasma Metabolomic Profiling of *P. falciparum* Infections in The Gambia**
613 (**A**) Region in The Gambia where plasma samples were taken from volunteers in neighboring
614 villages within a 5km radius (left). Overview of the change from high transmission to low
615 transmission months in The Gambia. Sample numbers are indicated by each month for
616 volunteers that had symptomatic or asymptomatic infections as well individuals with no
617 detected presence of *P. falciparum* (right). (**B**) Schematic showing the flow of the experimental
618 analysis for gas chromatography coupled with triple-quadrupole mass spectrometry (GC–
619 QqQ/MS) for widely targeted metabolites. (A, B) Figures created with BioRender.com (**C**)
620 Metabolite class enrichment for all 78 metabolites that passed quality control. (**D**) Pathway
621 enrichment analysis of the 78 metabolites used in analysis are shown with p-value and
622 enrichment ratio. (**E**) PCA plot for all 78 metabolites and all (n=199) plasma samples for the

three clinical conditions (symptomatic infections, asymptomatic infections, and uninfected negative).

Fig. S1: Additional information on samples used

(**A**) Parasitemia determined by qPCR for each of the conditions with available data, analyzed previously in [44]. Symptomatic October (n=7) and November (n=12), Asymptomatic October (n=24), November (n=22), December (n=44), January (n=42), February (n=29), March (n=3), April (n=4), and May (n=21). The center line represents the mean with error bars showing standard deviation. Statistical significance was determined by unpaired t-test comparing symptomatic infections to asymptomatic infections in the same months (** October p = 0.0085, November p = 0.0038). (**B**) Sample distribution for all conditions in each month. The median age in years is shown as well as the distribution by sex for males and females. **(C)** Age distribution for all individuals from each of the conditions in each month. Grey boxes represent the mean age with error bars showing standard deviation. (**D**) Heatmap for all 78 metabolites and (n=199) plasma samples with hierarchical clustering illustrating the changes in metabolite abundances according to the median of each metabolite. Rows are metabolites, columns are samples. Heatmap data are log2 normalized and centered around the average abundance computed from all the samples for each metabolite. Red/green colors are ion signal higher/lower than average. Samples and metabolites are clustered following the ward.D2 algorithm, with Euclidean distance.

Fig. 2: Metabolites associated with seasonality and severity.

(**A**) Volcano plot showing metabolites that had significantly increased levels in asymptomatic infections during the high transmission season (October) compared to the low transmission season (May). The median difference is plotted on the x-axis and the $-\log_{10}$ (FDR adjusted p-value) is plotted on the y-axis. Red colored circles represent significant metabolites with FDR ≤ 0.05 **(B)** Volcano plot showing metabolites that had significantly increased levels in symptomatic infections during the high transmission season (October, November) compared to asymptomatic infection during the high transmission season (October, November). The $\log_2$(Odds ratio) is plotted on the x-axis and the $-\log_{10}$ (FDR adjusted p-value) is plotted on the y-axis. Red colored circles represent significant metabolites with FDR ≤ 0.05 **(C)** Heatmap from MS analysis showing metabolites that varied based on severity and seasonality. All (n=199) samples, months, and conditions are included. Columns are metabolites, rows are

656 samples. Heatmap data are log2 normalized (within a range of [-2]-[2]) and centered around
657 the average abundance computed from all the samples for each metabolite. Red/green colors
658 are ion signal higher/lower than average. Samples and metabolites are clustered following the
659 ward.D2 algorithm, with Euclidean distance. **(C)**
660
661 **Fig. S2: Taurine levels rise in multiple individuals during the low transmission period.**
662 **(A)** Spaghetti plots showing taurine and allantoin levels in individuals (n=16) with persistent
663 infections who had samples taken for consecutive months during the low transmission period
664 (December-May). Values plotted are relative abundance determined from the MS analysis. **(B)**
665 Scatter plot showing relative abundance levels, determine by MS metabolomic analysis, of
666 taurine in symptomatic infections, asymptomatic infections, and uninfected negative
667 individuals. High transmission (HT) and low transmission (LT) months are labeled. Error bars
668 represent standard deviation and mean values are represented in shaded boxes for all conditions
669 and corresponding months.
670
671 **Fig. 3: Taurine markedly reduces iRBC adhesion**
672 (**A**) iRBC adhesion binding assays showing 3D7 iRBCs binding to CD36. Parasites have been
673 incubated for 30 hours in [0.04mM] methionine or increasing concentrations of taurine.
674 Additionally, parasites were incubated for one hour in [0.16mM] taurine. Data is expressed as
675 the percentage of iRBCs binding ±SD per mm^2 for each condition compared to control, with
676 the median represented at the center line. Results shown are three biological replicates (n=3)
677 from duplicate technical replicates. Statistical significance was determined by paired t-test (*
678 $p = 0.0305$ and 0.0152, **** $p < 0.0001$). (**B**) Representative iRBC adhesion assay images are
679 shown for control and supplementation of taurine physiological concentration [0.16mM]. (**C**)
680 EPCR binding assay of Itvar19 FCR3 iRBCs in the presence of [0.16mM] taurine and
681 [0.64mM] taurine. Data is expressed as the percentage of iRBCs binding ±SD per mm^2 for each
682 condition compared to control, with the median represented at the center line. Results are from
683 a total of three biological replicates (n=3) done in duplicate. Statistical significance was
684 determined by paired t-test (* $p = 0.0264$, ** $p = 0.0045$).
685
686 **Fig. S3: Taurine reduces iRBC adhesion without affecting parasite growth**
687 (**A**) Five-day growth curve of 3D7 wild-type *P. falciparum* cultured under three conditions:
688 control, 0.16 mM taurine (physiological concentration), and 0.27 mM threonic acid
689 (physiological concentration). Error bars represent the standard deviation of three biological

690 replicates performed in triplicate with different donor blood (n = 3). (**B)** Replicate counts (n=3)
691 for adhesion assays from (Fig. 3A). Data is expressed as the number of bound 3D7 iRBCs per
692 mm^2 of coated receptor for each condition. **(C**) iRBC adhesion assays showing *P.*
693 *falciparum* 3D7 iRBCs binding to CD36 after 1-hour incubation with 0.27 mM threonic acid.
694 Data are presented as the percentage of iRBCs bound per mm^2 (±SD), relative to control;
695 median values are indicated by the center line. Results represent three biological replicates
696 (n = 3), each performed in duplicate. Statistical significance was determined by paired t-test (*
697 p = 0.0305 and 0.0152, **** p < 0.0001). NS indicates not significant. **(D)** iRBC adhesion
698 assays examining parasite FCR3 Itvar19 iRBCs binding to CD36, with or without pre-treatment
699 with [0.16mM] taurine for one hour before the binding assay [parasites were the same strain as
700 those used from (Fig. 3C)]. Data is expressed as the percentage of bound iRBCs ±SD per mm^2
701 for each condition compared to control, with the median represented at the center line. Results
702 are from a total of three biological replicates (n=3) done in duplicate. Statistical significance
703 was determined by paired t-test (*** p = 0.0003). (**E)** iRBC adhesion assays for NF54
704 VAR2CSA iRBCS binding to CSA for control and [0.64mM] taurine. Data is expressed as the
705 percentage of bound iRBCs ±SD per mm^2 for each condition compared to control, with the
706 median represented at the center line. Results are from a total of three biological replicates
707 (n=3) done in duplicate. Statistical significance was determined by paired t-test (* p = 0.0288).
708 **(F)** iRBC adhesion assays assessing 3D7 iRBCs binding to CD36 under control conditions and
709 with the addition of 10% human serum with or without [0.64mM] taurine supplementation.
710 Data is expressed as the percentage of bound iRBCs ±SD per mm^2 compared to control, with
711 the median represented at the center line. Results are from a total of three biological replicates
712 (n=3) done in duplicate. Statistical significance was determined by paired t-test (* p= 0.035,
713 ** p = 0.0066).
714
715 **Fig. 4: Taurine-Mediated Reversal of iRBC Receptor Binding and Inhibition of**
716 **Cytoadhesion to C32 Cells**
717 (**A**) Reversal of iRBC adhesion of 3D7 iRBCs bound to CD36, incubated with or without
718 [0.64mM] taurine. Data is expressed as the fold change of bound iRBCs ±SD per mm^2
719 compared to control, with the median represented at the center line. Results are from a total of
720 three biological replicates (n=3) done in duplicate. Statistical significance was determined by
721 paired t-test (*** p = 0.0009). (**B**) Reversible iRBC adhesion assays for FCR3 Itvar19 parasites
722 bound to EPCR incubated with or without [0.64mM] taurine. Data is expressed as the fold
723 change of bound iRBCs ±SD per mm^2 compared to control, with the median represented at the

724 center line. Results are from a total of three biological replicates (n=3) done in duplicate.
725 Statistical significance was determined by paired t-test (** p = 0.0179). (**C**) Cytoadhesion
726 assays measuring *P. falciparum* FCR3 parasite strain binding to human C32 melanoma cells
727 expressing CD36 and ICAM-1 under control conditions and with increasing taurine
728 concentrations (0.16 mM, 0.64 mM, 0.93 mM). Data is expressed as the fold change of bound
729 iRBCs per mm^2 of confluent C32 cells (±SD), with medians indicated by center lines. Results
730 represent three biological replicates (n = 3), each in duplicate. Statistical significance was
731 determined by paired t-test (* p = 0.0231, ** p = 0.0076); NS = not significant. (**D**)
732 Representative field of cytoadhesion assay from (Fig. 4C).
733

734 **Fig. S4: Taurine does not alter PfEMP1 surface expression**

735 **(A)** FACS analysis for surface expression of PfEMP1 from parasites, incubated with or without
736 [0.64mM] taurine, from a total of three biological replicates (n=3) done in duplicate using an
737 antibody against *var19* PfEMP1. Statistical significance was determined by paired t-test (NS
738 indicates not significant). (**B**) Flow-cytometry gating strategy. Gating hierarchy for a
739 representative sample. From left to right: (a) In the FSC-A versus SSC-A plot, the cloud of
740 RBC events is identified. (b) Among the RBCs, in the FSC-A versus FSC-H plot, singlets
741 (single cell signals) are distinguished. (c) Among the singlets, the APC-A histogram is used to
742 identify iRBCs. (d) Finally, in the PE-A channel, cells expressing var19 on their surface are
743 identified based on PE-A labelling. **(C)** Flow cytometry analysis of FCR3 Var19 infected red
744 blood cells. Percentage of Var19 expression on the cell surface without or with [0.64mM]
745 taurine supplementation (negative controls included). Histogram legends for the expression
746 data and the percentage of Var19 expression on the surface with the geometric mean are shown.
747 Results are from three biological replicates (n=3). **(D)** iRBC adhesion assays assessing 3D7
748 parasite binding to CD36 under control conditions and with CD36 pre-incubated with
749 [0.16mM] taurine. Data is expressed as the percentage of bound iRBCs ±SD per mm^2 compared
750 to control, with the median represented at the center line. Results are from a total of three
751 biological replicates (n=3) done in duplicate. Statistical significance was determined by paired
752 t-test (NS indicates not significant). **(E)** Cytoadhesion assays measuring 3D7 iRBCs binding
753 to human C32 melanoma cells expressing CD36 and ICAM-1 under control conditions and
754 [0.93mM] taurine. Replicate counts (n=2) for cytoadhesion assays. Data is expressed as the
755 number of bound iRBCs per mm^2 of confluent C32 cells for each condition (±SD), with

756 medians indicated by center lines. (**F**) Representative field of cytoadhesion assay from (Fig.
757 S4E).
758

759 **References**

760 1. W.H.O. World Malaria Report 2023. (2023).
761 2. Wahlgren, M., Goel, S. & Akhouri, R. R. Variant surface antigens of Plasmodium
762 falciparum and their roles in severe malaria. *Nat Rev Microbiol* (2017).
763 3. Miller, L. H., Baruch, D. I., Marsh, K. & Doumbo, O. K. The pathogenic basis of
764 malaria. *Nature* **415**, 673–679 (2002).
765 4. Scherf, A., Lopez-Rubio, J. J. & Riviere, L. Antigenic variation in Plasmodium
766 falciparum. *Annu Rev Microbiol* **62**, 445–470 (2008).
767 5. Deitsch, K. W. & Dzikowski, R. Variant Gene Expression and Antigenic Variation by
768 Malaria Parasites. *Annu Rev Microbiol* **71**, 625–641 (2017).
769 6. Baruch, D. I. *et al.* Cloning the P. falciparum gene encoding PfEMP1, a malarial variant
770 antigen and adherence receptor on the surface of parasitized human erythrocytes. *Cell* **82**,
771 77–87 (1995).
772 7. Smith, J. D. *et al.* Switches in expression of plasmodium falciparum var genes correlate
773 with changes in antigenic and cytoadherent phenotypes of infected erythrocytes. *Cell* **82**,
774 101–110 (1995).
775 8. Su, X. Z. *et al.* The large diverse gene family var encodes proteins involved in
776 cytoadherence and antigenic variation of plasmodium falciparum-infected erythrocytes.
777 *Cell* **82**, 89–100 (1995).
778 9. Gardner, M. J. *et al.* Genome sequence of the human malaria parasite Plasmodium
779 falciparum. *Nature* **419**, 498–511 (2002).

780 10. Smith, J. D., Rowe, J. A., Higgins, M. K. & Lavstsen, T. Malaria's deadly grip:
781 cytoadhesion of Plasmodium falciparum-infected erythrocytes: Plasmodium falciparum
782 cytoadhesion and var genes. *Cell Microbiol* **15**, 1976–1983 (2013).
783 11. Robinson, B. A., Welch, T. L. & Smith, J. D. Widespread functional specialization of
784 Plasmodium falciparum erythrocyte membrane protein 1 family members to bind CD36
785 analysed across a parasite genome. *Mol Microbiol* **47**, 1265–1278 (2003).
786 12. Hsieh, F.-L. *et al.* The structural basis for CD36 binding by the malaria parasite. *Nat*
787 *Commun* **7**, 12837 (2016).
788 13. Turner, L. *et al.* Severe malaria is associated with parasite binding to endothelial protein
789 C receptor. *Nature* **498**, 502–505 (2013).
790 14. Lau, C. K. Y. *et al.* Structural Conservation Despite Huge Sequence Diversity Allows
791 EPCR Binding by the PfEMP1 Family Implicated in Severe Childhood Malaria. *Cell*
792 *Host & Microbe* **17**, 118–129 (2015).
793 15. Urban, B. C. *et al.* Plasmodium falciparum-infected erythrocytes modulate the maturation
794 of dendritic cells. *Nature* **400**, 73–77 (1999).
795 16. Serghides, L., Smith, T. G., Patel, S. N. & Kain, K. C. CD36 and malaria: friends or foes?
796 *Trends Parasitol* **19**, 461–469 (2003).
797 17. Avril, M. *et al.* A restricted subset of var genes mediates adherence of Plasmodium
798 falciparum-infected erythrocytes to brain endothelial cells. *Proc Natl Acad Sci U S A* **109**,
799 E1782-1790 (2012).
800 18. Claessens, A. *et al.* A subset of group A-like var genes encodes the malaria parasite
801 ligands for binding to human brain endothelial cells. *Proc Natl Acad Sci U S A* **109**,
802 E1772-1781 (2012).

803 19. Lavstsen, T. *et al.* Plasmodium falciparum erythrocyte membrane protein 1 domain
804 cassettes 8 and 13 are associated with severe malaria in children. *Proc Natl Acad Sci U S*
805 *A* **109**, E1791-1800 (2012).
806 20. Tuikue Ndam, N. *et al.* Parasites Causing Cerebral Falciparum Malaria Bind Multiple
807 Endothelial Receptors and Express EPCR and ICAM-1-Binding PfEMP1. *The Journal of*
808 *Infectious Diseases* **215**, 1918–1925 (2017).
809 21. Lennartz, F. *et al.* Structure-Guided Identification of a Family of Dual Receptor-Binding
810 PfEMP1 that Is Associated with Cerebral Malaria. *Cell Host Microbe* **21**, 403–414
811 (2017).
812 22. Babbitt, S. E. *et al.* Plasmodium falciparum responds to amino acid starvation by entering
813 into a hibernatory state. *Proc Natl Acad Sci U S A* **109**, E3278-3287 (2012).
814 23. Schneider, V. M. *et al.* The human malaria parasite Plasmodium falciparum can sense
815 environmental changes and respond by antigenic switching. *Proc Natl Acad Sci U S A*
816 **120**, e2302152120 (2023).
817 24. Marreiros, I. M. *et al.* A non-canonical sensing pathway mediates Plasmodium adaptation
818 to amino acid deficiency. *Commun Biol* **6**, 205 (2023).
819 25. Brancucci, N. M. B. *et al.* Lysophosphatidylcholine Regulates Sexual Stage
820 Differentiation in the Human Malaria Parasite Plasmodium falciparum. *Cell* **171**, 1532-
821 1544.e15 (2017).
822 26. Diffendall, G. *et al.* RNA polymerase III is involved in regulating Plasmodium
823 falciparum virulence. *Elife* **13**, RP95879 (2024).
824 27. Mancio-Silva, L. *et al.* Nutrient sensing modulates malaria parasite virulence. *Nature*
825 **547**, 213–216 (2017).
826 28. Babiker, H. A., Abdel-Muhsin, A. M., Ranford-Cartwright, L. C., Satti, G. & Walliker,
827 D. Characteristics of Plasmodium falciparum parasites that survive the lengthy dry season

828 in eastern Sudan where malaria transmission is markedly seasonal. *Am J Trop Med Hyg*
829 **59**, 582–590 (1998).
830 29. Andrade, C. M., Fleckenstein, H. & Thomson-Luque, R. Increased circulation time of
831 Plasmodium falciparum underlies persistent asymptomatic infection in the dry season.
832 *Nat Med* **26**, 1929–1940 (2020).
833 30. Portugal, S. *et al.* Treatment of Chronic Asymptomatic Plasmodium falciparum Infection
834 Does Not Increase the Risk of Clinical Malaria Upon Reinfection. *Clin Infect Dis* **64**,
835 645–653 (2017).
836 31. Thomson-Luque, R. *et al.* Plasmodium falciparum transcription in different clinical
837 presentations of malaria associates with circulation time of infected erythrocytes. *Nat*
838 *Commun* **12**, 4711 (2021).
839 32. Andrade, C. M. *et al.* Infection length and host environment influence on Plasmodium
840 falciparum dry season reservoir. *EMBO Mol Med* **16**, 2349–2375 (2024).
841 33. Fogang, B. *et al.* Asymptomatic Plasmodium falciparum carriage at the end of the dry
842 season is associated with subsequent infection and clinical malaria in Eastern Gambia.
843 *Malar J* **23**, 22 (2024).
844 34. Guery, M.-A. *et al.* Household clustering and seasonal genetic variation of Plasmodium
845 falciparum at the community-level in The Gambia. *eLife* **13**, RP103047 (2025).
846 35. Surowiec, I. *et al.* Metabolic Signature Profiling as a Diagnostic and Prognostic Tool in
847 Pediatric Plasmodium falciparum Malaria. *Open Forum Infectious Diseases* **2**, ofv062
848 (2015).
849 36. Beri, D. *et al.* Insights into physiological roles of unique metabolites released from
850 Plasmodium-infected RBCs and their potential as clinical biomarkers for malaria. *Sci Rep*
851 **9**, 2875 (2019).

852 37. Leopold, S. J. *et al.* Identifying the Components of Acidosis in Patients With Severe
853 Plasmodium falciparum Malaria Using Metabolomics. *The Journal of Infectious Diseases*
854 **219**, 1766–1776 (2019).
855 38. Lakshmanan, V. *et al.* Metabolomic analysis of patient plasma yields evidence of plant-
856 like α-linolenic acid metabolism in Plasmodium falciparum. *J Infect Dis* **206**, 238–248
857 (2012).
858 39. Abdrabou, W. *et al.* Metabolome modulation of the host adaptive immunity in human
859 malaria. *Nat Metab* **3**, 1001–1016 (2021).
860 40. Collins, K. A. *et al.* A Cohort Study on the Duration of Plasmodium falciparum
861 Infections During the Dry Season in The Gambia. *J Infect Dis* **226**, 128–137 (2022).
862 41. Huxtable, R. J. Physiological actions of taurine. *Physiol Rev* **72**, 101–163 (1992).
863 42. Debierre-Grockiego, F. *et al.* Fatty acids from Plasmodium falciparum down-regulate the
864 toxic activity of malaria glycosylphosphatidylinositols. *Infect Immun* **74**, 5487–5496
865 (2006).
866 43. Sasi, P. *et al.* Metabolic acidosis and other determinants of hemoglobin-oxygen
867 dissociation in severe childhood Plasmodium falciparum malaria. *Am J Trop Med Hyg*
868 **77**, 256–260 (2007).
869 44. Wei, Z. *et al.* β-hydroxybutyrate inhibits Plasmodium falciparum development and
870 confers protection against malaria in mice. *Nat Metab* **7**, 1330–1343 (2025).
871 45. Baliou, S. *et al.* Protective role of taurine against oxidative stress (Review). *Mol Med Rep*
872 **24**, 605 (2021).
873 46. Li, X. *et al.* Taurine potentiates artemisinin efficacy against malaria by modulating the
874 immune response in Plasmodium berghei-infected mice. *Parasit Vectors* **17**, 493 (2024).
875 47. Shi, X. *et al.* Vitamin C Inhibits Blood-Stage Plasmodium Parasites via Oxidative Stress.
876 *Front Cell Dev Biol* **9**, 639944 (2021).

877 48. Trautwein, E. & Hayes, K. Taurine concentrations in plasma and whole blood in humans:
878 estimation of error from intra- and interindividual variation and sampling technique. *The*
879 *American Journal of Clinical Nutrition* **52**, 758–764 (1990).
880 49. Wang, H., Hu, P. & Jiang, J. Pharmacokinetics and safety of calcium L-threonate in
881 healthy volunteers after single and multiple oral administrations. *Acta Pharmacol Sin* **32**,
882 1555–1560 (2011).
883 50. Rajapandi, T., Ackie, K. & Rajeev Hegde, K. Anti-plasmodial Activity of a Non-protein
884 Amino Acid Taurine. *BS* **5**, 34 (2019).
885 51. Ghandforoush-Sattari, M., Mashayekhi, S., Krishna, C. V., Thompson, J. P. & Routledge,
886 P. A. Pharmacokinetics of Oral Taurine in Healthy Volunteers. *Journal of Amino Acids*
887 **2010**, 1–5 (2010).
888 52. Garlick, P. J. Toxicity of Methionine in Humans. *The Journal of Nutrition* **136**, 1722S-
889 1725S (2006).
890 53. Srivastava, A. *et al.* Var2CSA Minimal CSA Binding Region Is Located within the N-
891 Terminal Region. *PLoS ONE* **6**, e20270 (2011).
892 54. Nunes-Silva, S. *et al.* Beninese children with cerebral malaria do not develop humoral
893 immunity against the IT4-VAR19-DC8 PfEMP1 variant linked to EPCR and brain
894 endothelial binding. *Malar J* **14**, 493 (2015).
895 55. Viebig, N. K. *et al.* A single member of the *Plasmodium falciparum var* multigene family
896 determines cytoadhesion to the placental receptor chondroitin sulphate A. *EMBO Reports*
897 **6**, 775–781 (2005).
898 56. Nacer, A. *et al.* Clag9 is not essential for PfEMP1 surface expression in non-cytoadherent
899 Plasmodium falciparum parasites with a chromosome 9 deletion. *PLoS One* **6**, e29039
900 (2011).

901 57. Schmidt, J. A. *et al.* Plasmodium Falciparum Malaria. *J. Clin. Invest.* **70**, 379–386
902 (1982).
903 58. Ho, M. *et al.* Clinical correlates of in vitro Plasmodium falciparum cytoadherence. *Infect*
904 *Immun* **59**, 873–878 (1991).
905 59. Ockenhouse, C. F. *et al.* Molecular basis of sequestration in severe and uncomplicated
906 Plasmodium falciparum malaria: differential adhesion of infected erythrocytes to CD36
907 and ICAM-1. *J Infect Dis* **164**, 163–169 (1991).
908 60. Beck, J. R. & Ho, C.-M. Transport mechanisms at the malaria parasite-host cell interface.
909 *PLoS Pathog* **17**, e1009394 (2021).
910 61. Jabre, I. *et al.* Histone lactylation: a new epigenetic mark in the malaria parasite
911 *Plasmodium*. Preprint at https://doi.org/10.1101/2024.08.19.608576 (2024).
912 62. Merrick, C. J. *et al.* Epigenetic dysregulation of virulence gene expression in severe
913 Plasmodium falciparum malaria. *J Infect Dis* **205**, 1593–1600 (2012).
914 63. Stacy, A. *et al.* Infection trains the host for microbiota-enhanced resistance to pathogens.
915 *Cell* **184**, 615-627.e17 (2021).
916 64. Reyes, R. A. *et al.* Broadly inhibitory antibodies to severe malaria virulence proteins.
917 *Nature* **636**, 182–189 (2024).
918 65. Schaffer, S. & Kim, H. W. Effects and Mechanisms of Taurine as a Therapeutic Agent.
919 *Biomolecules & Therapeutics* **26**, 225–241 (2018).
920 66. Grajeda-Iglesias, C. *et al.* Oral administration of Akkermansia muciniphila elevates
921 systemic antiaging and anticancer metabolites. *Aging (Albany NY)* **13**, 6375–6405 (2021).
922 67. Durand, S. *et al.* The intracellular metabolome of starving cells. in *Methods in Cell*
923 *Biology* vol. 164 137–156 (Elsevier, 2021).

924 68. Lopez-Rubio, J. J., Mancio-Silva, L. & Scherf, A. Genome-wide analysis of
925 heterochromatin associates clonally variant gene regulation with perinuclear repressive
926 centers in malaria parasites. *Cell Host Microbe* **5**, 179–190 (2009).
927 69. Vembar, S. S., Macpherson, C. R., Sismeiro, O., Coppée, J. Y. & Scherf, A. The pfalba1
928 rna-binding protein is an important regulator of translational timing in plasmodium
929 falciparum blood stages. *Genome Biol* **16**, (2015).
930 70. Fried, M. *et al.* Multilaboratory approach to preclinical evaluation of vaccine
931 immunogens for placental malaria. *Infect Immun* **81**, 487–495 (2013).
932 71. Bryant, J. M. *et al.* Crispr/cas9 genome editing reveals that the intron is not essential for
933 var2csa gene activation or silencing in plasmodium falciparum. *MBio* **8**, (2017).
934 72. Nacer, A. *et al.* clag9 Is Not Essential for PfEMP1 Surface Expression in Non-
935 Cytoadherent Plasmodium falciparum Parasites with a Chromosome 9 Deletion. *PLoS*
936 *ONE* **6**, e29039 (2011).
937

938 **Acknowledgments:** We thank Jessica Bryant for critical reading of this manuscript. We
939 thank Célia Peuziat and Sooraj Shivakumar for technical assistance with this project.
940

941 **Funding:** This work was supported by funding to AS from the Laboratoire d'Excellence
942 (LabEx) ParaFrap (ANR-11-LABX- 0024), ANR VAR2PTM (ANR-22-CE15-0023).
943 This work was also supported by funding to AC from MRC/LSHTM fellowship,
944 the Agence Nationale de la Recherche (ANR-18-CE15-0009-01). This work was
945 additionally supported by funding to BG from the Fondation pour la Recherche
946 Médicale (Equipe FRM EQU202203014741).
947

948 **Author contributions:**
949 Conceptualization: GD, AS
950 Methodology: GD, PM, PC

Investigation: GD, PM, PC, BF, FA, DD, SD

Visualization: GD

Funding acquisition: AS, AC, BG

Project administration: GD, AS

Supervision: AS, AC, BG

Writing – original draft: GD, AS

Writing – review & editing: GD, AS, AC, BG

Competing interests:

The funders had no role in the study design, data collection, and interpretation or decision to submit the work for publication. The authors declare that they have no conflict of interest.

Data and materials availability: All data are available in the main text or the supplementary materials.

Figure 1

A

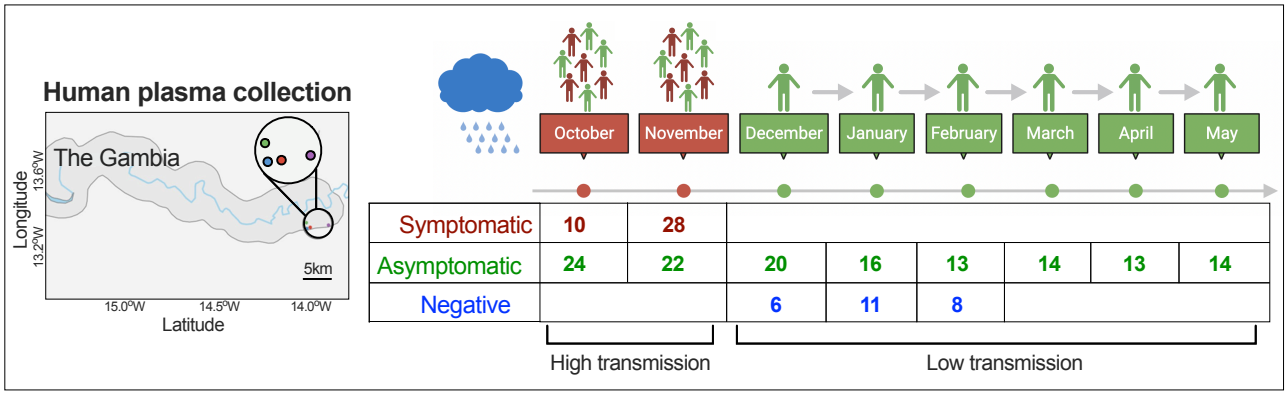

B

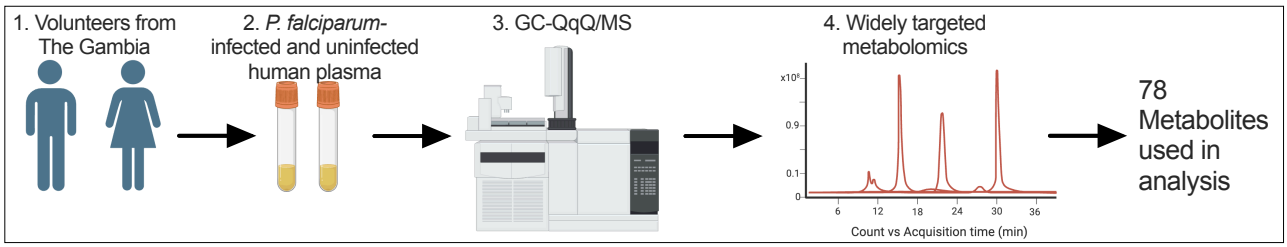

C

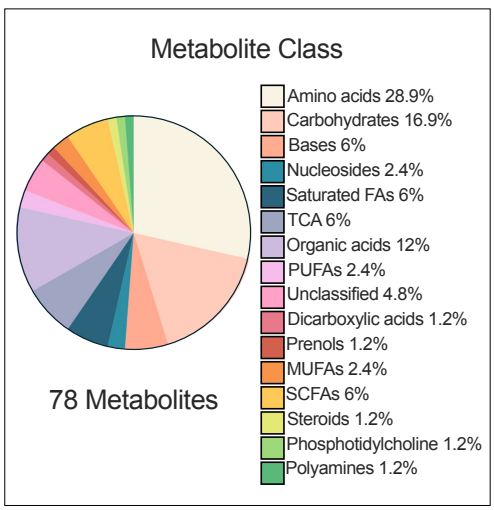

D

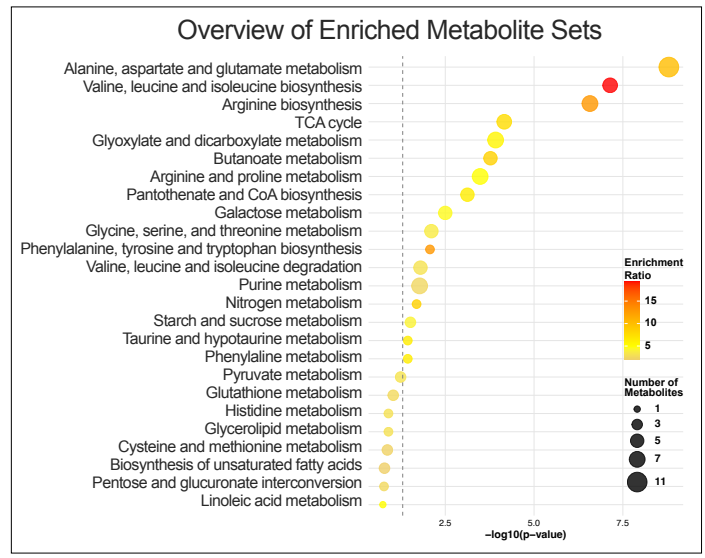

E

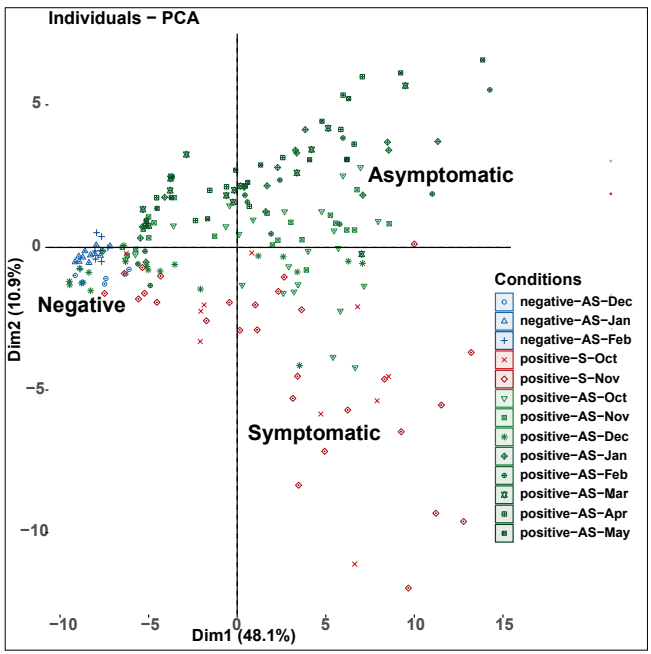

Figure 2

A

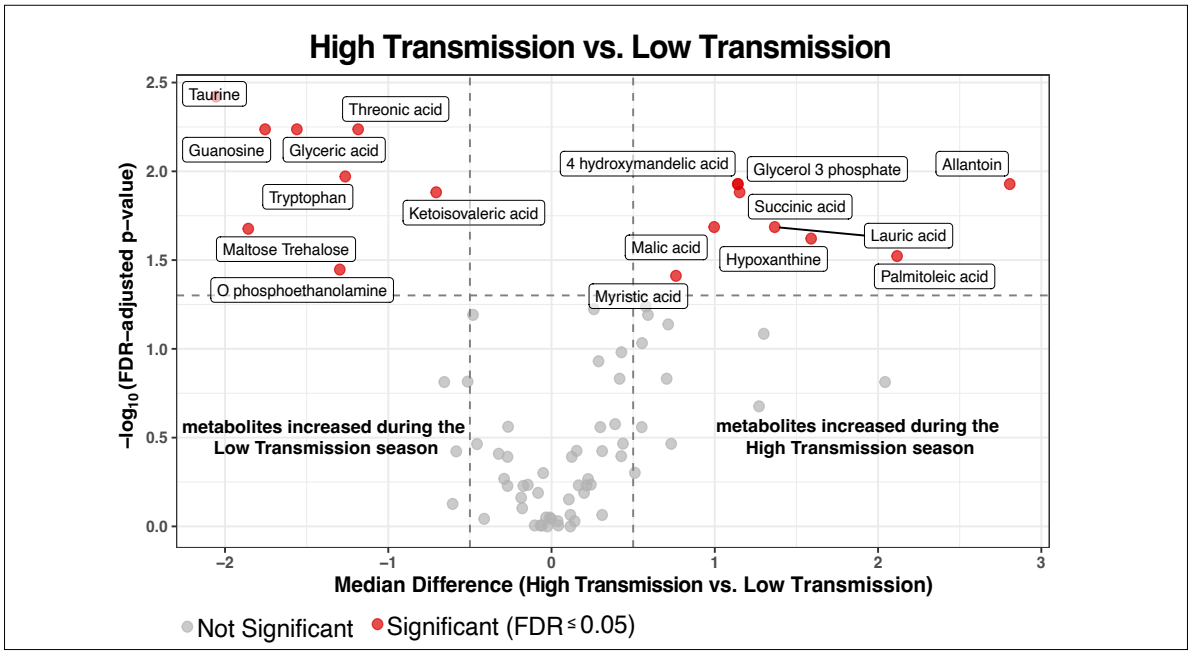
High Transmission vs. Low Transmission
Taurine
Threonic acid
Guanosine
Glyceric acid
Tryptophan
Ketoisovaleric acid
Maltose Trehalose
O phosphoethanolamine
4 hydroxymandelic acid
Glycerol 3 phosphate
Allantoin
Succinic acid
Lauric acid
Malic acid
Hypoxanthine
Palmitoleic acid
Myristic acid
metabolites increased during the Low Transmission season
metabolites increased during the High Transmission season
−log10 (FDR−adjusted p−value)
Median Difference (High Transmission vs. Low Transmission)
Not Significant
Significant (FDR ≤ 0.05)

B

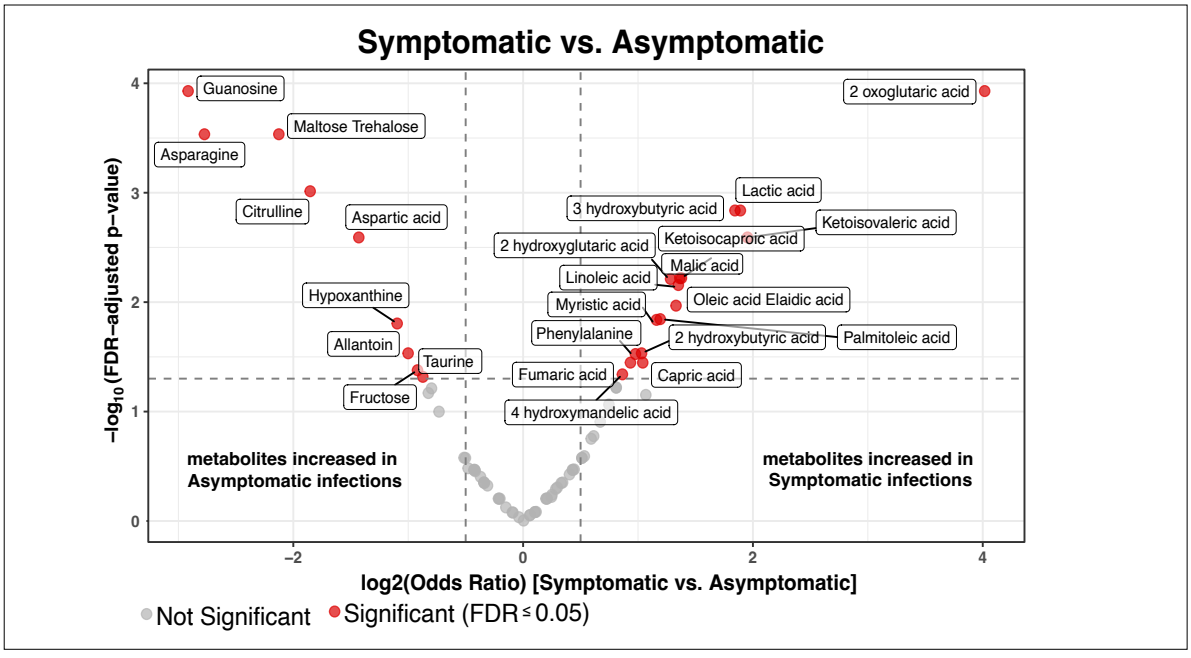
Symptomatic vs. Asymptomatic
Guanosine
Maltose Trehalose
Asparagine
Citrulline
Aspartic acid
Hypoxanthine
Allantoin
Taurine
Fructose
2 oxoglutaric acid
Lactic acid
3 hydroxybutyric acid
Ketoisovaleric acid
Ketoisocaproic acid
2 hydroxyglutaric acid
Malic acid
Linoleic acid
Oleic acid Elaidic acid
Myristic acid
Phenylalanine
2 hydroxybutyric acid
Palmitoleic acid
Fumaric acid
Capric acid
4 hydroxymandelic acid
metabolites increased in Asymptomatic infections
metabolites increased in Symptomatic infections
−log10 (FDR−adjusted p−value)
log2(Odds Ratio) [Symptomatic vs. Asymptomatic]
Not Significant
Significant (FDR ≤ 0.05)

C

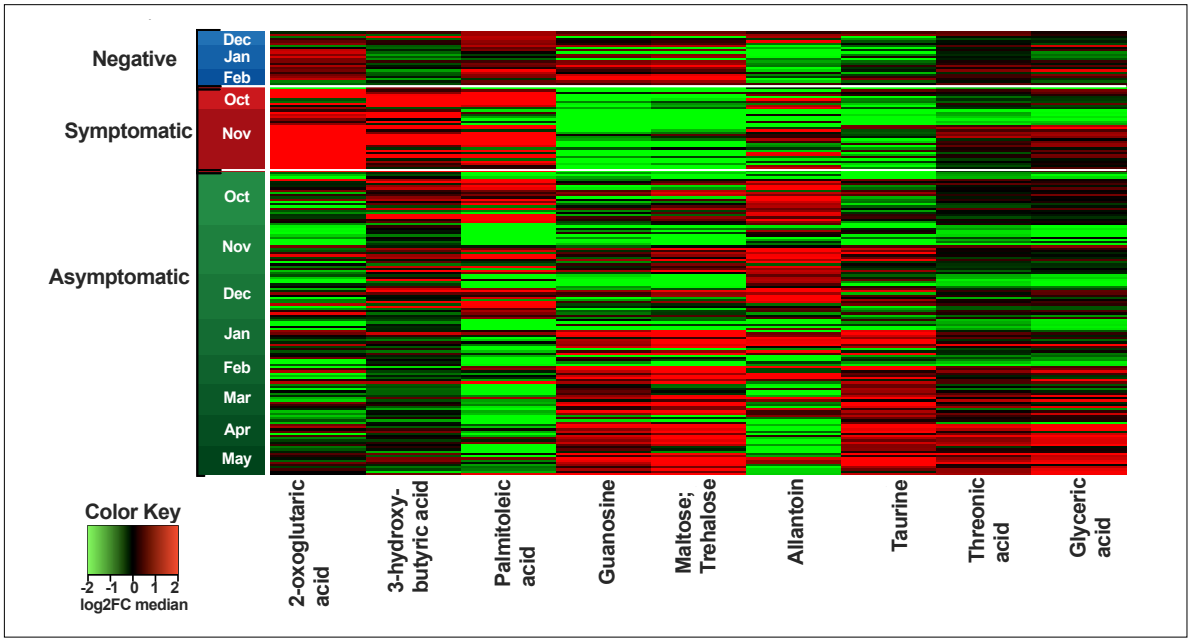
Negative
Symptomatic
Asymptomatic
Dec
Jan
Feb
Oct
Nov
Oct
Nov
Dec
Jan
Feb
Mar
Apr
May
Color Key
-2 -1 0 1 2
log2FC median
2-oxoglutaric acid
3-hydroxy-butyric acid
Palmitoleic acid
Guanosine
Maltose; Trehalose
Allantoin
Taurine
Threonic acid
Glyceric acid

Figure 3

A

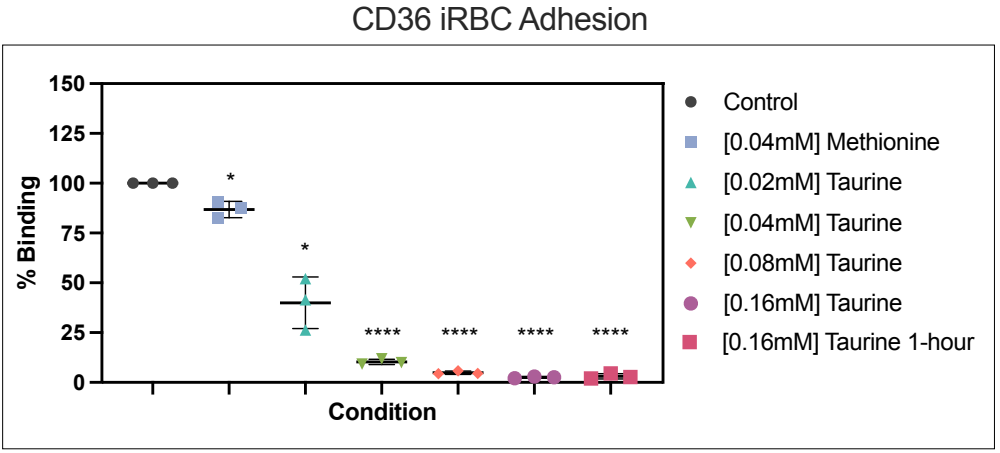
CD36 iRBC Adhesion
% Binding
150
125
100
75
50
25
0
*
*
****
****
****
****
Condition
Control
[0.04mM] Methionine
[0.02mM] Taurine
[0.04mM] Taurine
[0.08mM] Taurine
[0.16mM] Taurine
[0.16mM] Taurine 1-hour

B

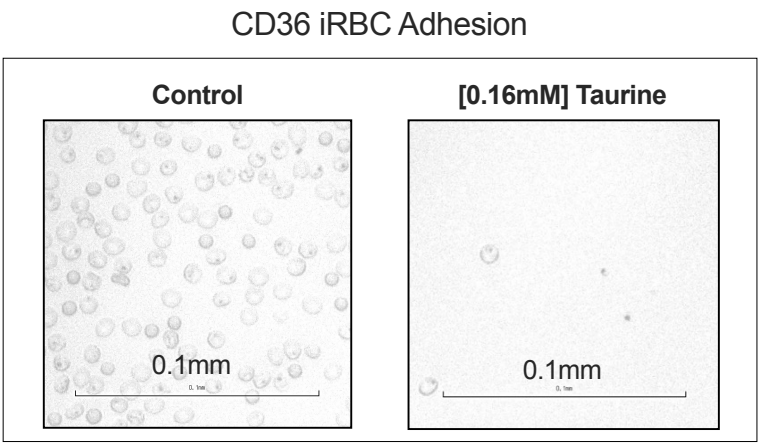
CD36 iRBC Adhesion
Control
[0.16mM] Taurine
0.1mm
0.1mm

C

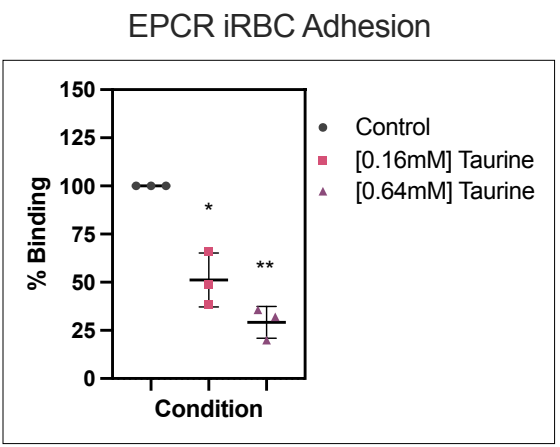
EPCR iRBC Adhesion
% Binding
150
125
100
75
50
25
0
*
**
Condition
Control
[0.16mM] Taurine
[0.64mM] Taurine

Figure 4

A

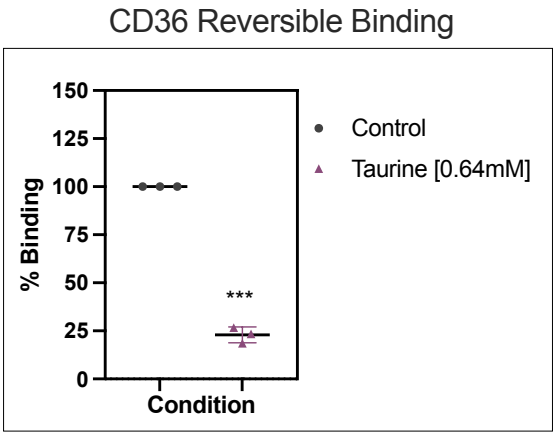

B

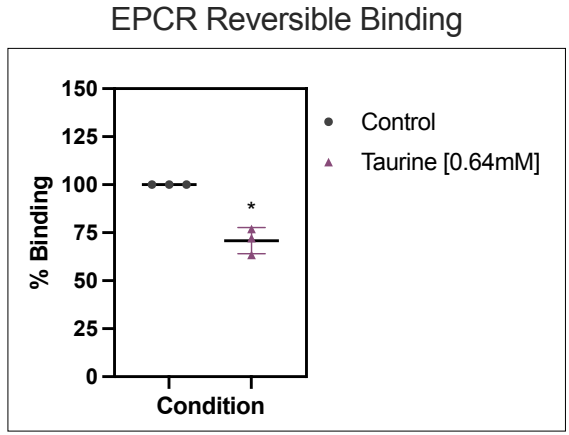

C

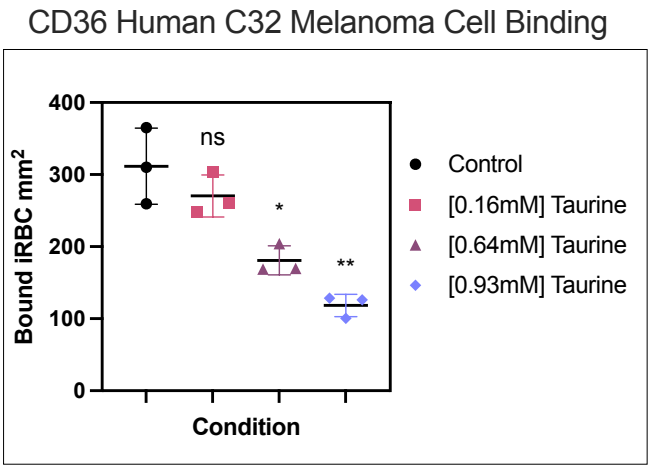

D

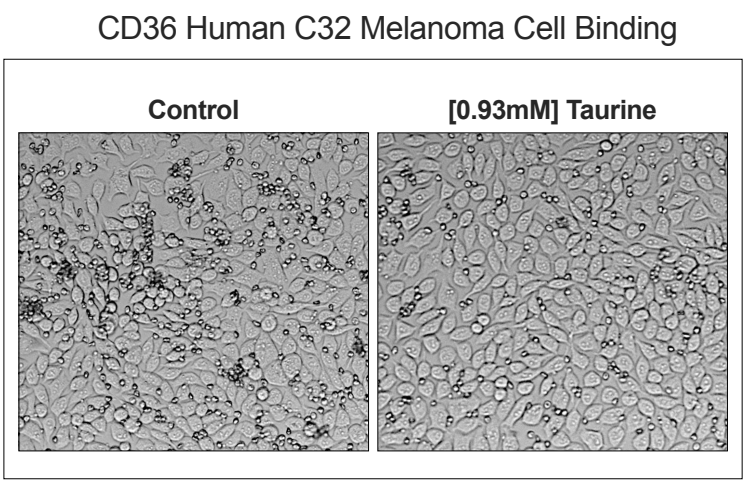

Figure S1

A

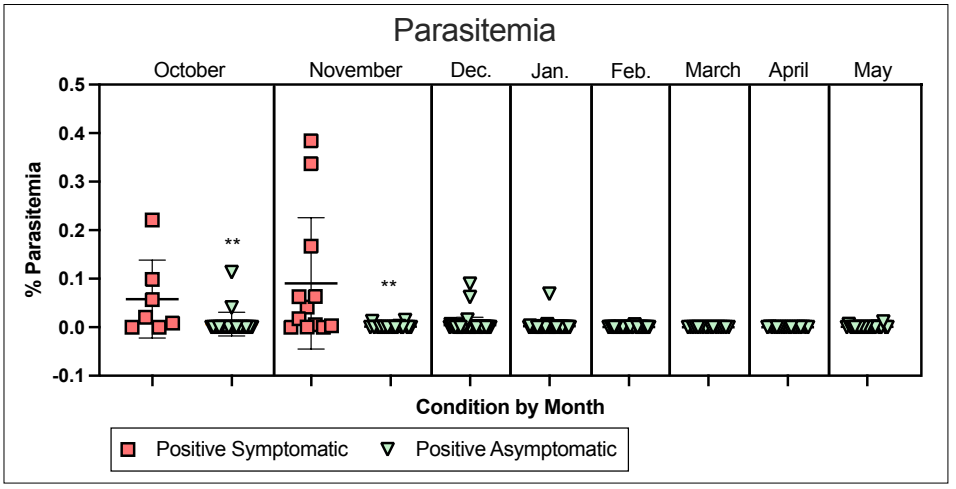

B

Sample Distribution

Month	Condition	Median age (years)	% Male	% Female
October	Positive Symptomatic	19	50%	50%
	Positive Asymptomatic	9.5	37.5%	62.5%
November	Positive Symptomatic	20.5	50%	50%
	Positive Asymptomatic	18	45.5%	54.5%
December	Negative	30	33.3%	66.7%
	Positive Asymptomatic	12.5	40%	60%
January	Negative	11	27.3%	72.7%
	Positive Asymptomatic	16.5	37.5%	62.5%
February	Negative	9	25%	75%
	Positive Asymptomatic	13	46.2%	53.8%
March	Positive Asymptomatic	14	42.9%	57.1%
April	Positive Asymptomatic	18	35.7%	64.3%
May	Positive Asymptomatic	18.5	35.7%	62.3%

C

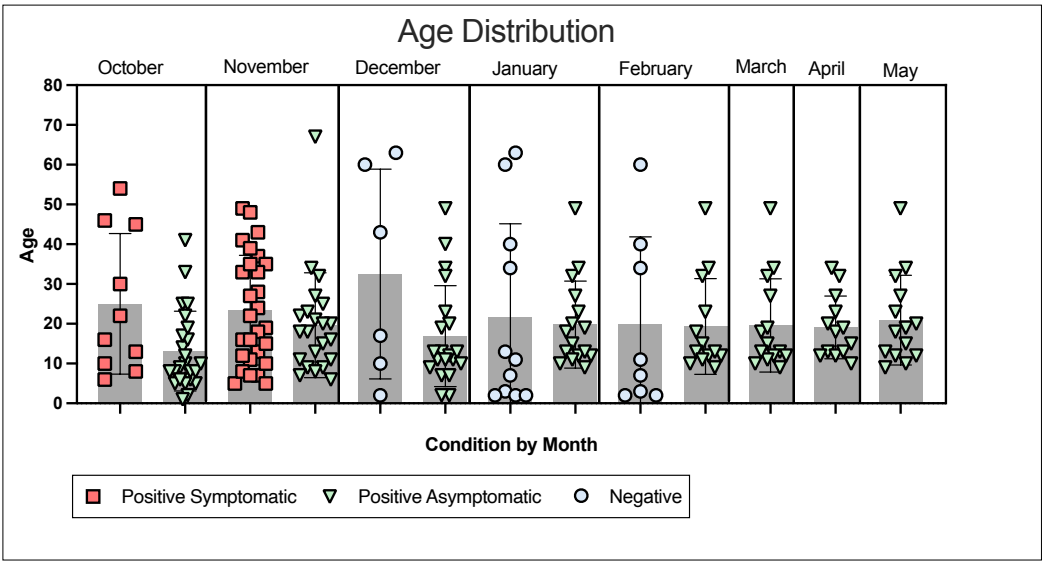

Figure S1
D

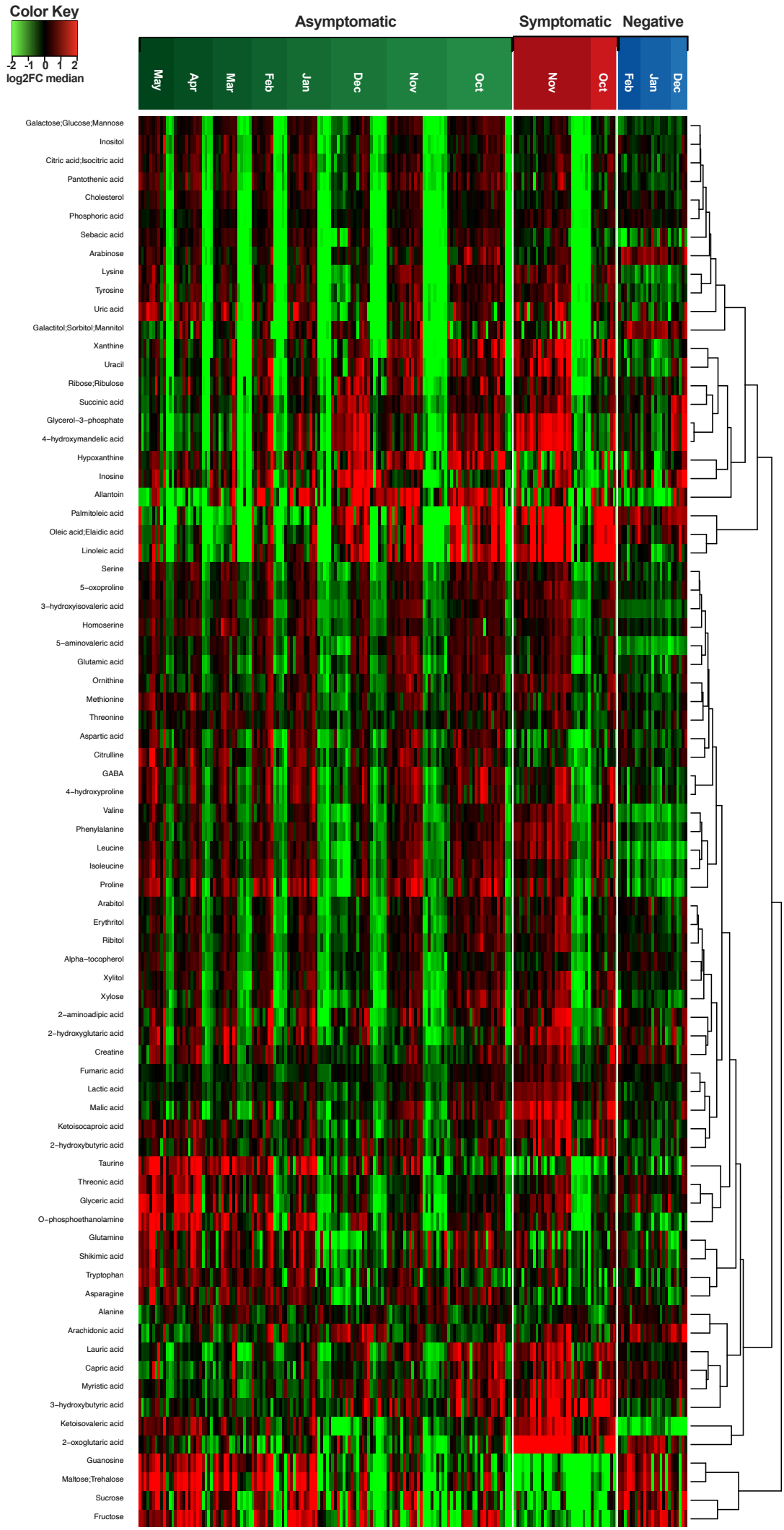
Color Key
-2 -1 0 1 2
log2FC median
Asymptomatic
Symptomatic
Negative
May
Apr
Mar
Feb
Jan
Dec
Nov
Oct
Nov
Oct
Feb
Jan
Dec
Galactose;Glucose;Mannose
Inositol
Citric acid;Isocitric acid
Pantothenic acid
Cholesterol
Phosphoric acid
Sebacic acid
Arabinose
Lysine
Tyrosine
Uric acid
Galactitol;Sorbitol;Mannitol
Xanthine
Uracil
Ribose;Ribulose
Succinic acid
Glycerol−3−phosphate
4−hydroxymandelic acid
Hypoxanthine
Inosine
Allantoin
Palmitoleic acid
Oleic acid;Elaidic acid
Linoleic acid
Serine
5−oxoproline
3−hydroxyisovaleric acid
Homoserine
5−aminovaleric acid
Glutamic acid
Ornithine
Methionine
Threonine
Aspartic acid
Citrulline
GABA
4−hydroxyproline
Valine
Phenylalanine
Leucine
Isoleucine
Proline
Arabitol
Erythritol
Ribitol
Alpha−tocopherol
Xylitol
Xylose
2−aminoadipic acid
2−hydroxyglutaric acid
Creatine
Fumaric acid
Lactic acid
Malic acid
Ketoisocaproic acid
2−hydroxybutyric acid
Taurine
Threonic acid
Glyceric acid
O−phosphoethanolamine
Glutamine
Shikimic acid
Tryptophan
Asparagine
Alanine
Arachidonic acid
Lauric acid
Capric acid
Myristic acid
3−hydroxybutyric acid
Ketoisovaleric acid
2−oxoglutaric acid
Guanosine
Maltose;Trehalose
Sucrose
Fructose

Figure S2

A

Longitudinal metabolite levels in the same individuals (n=16)

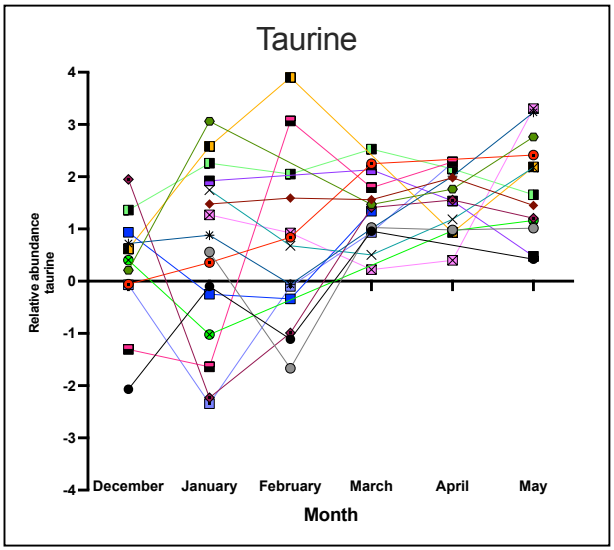

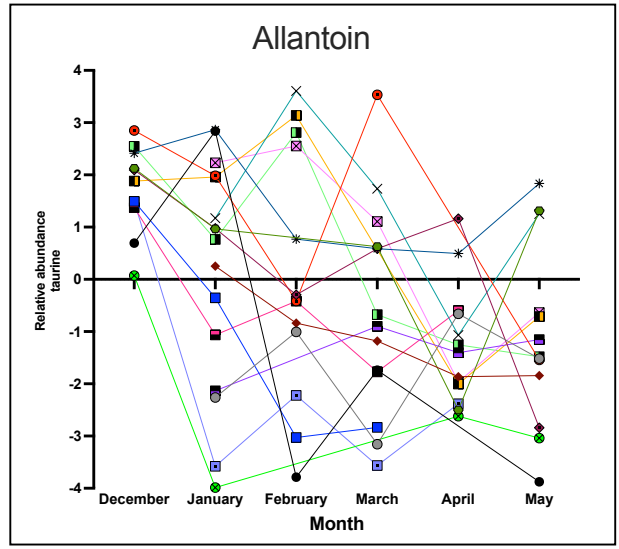

B

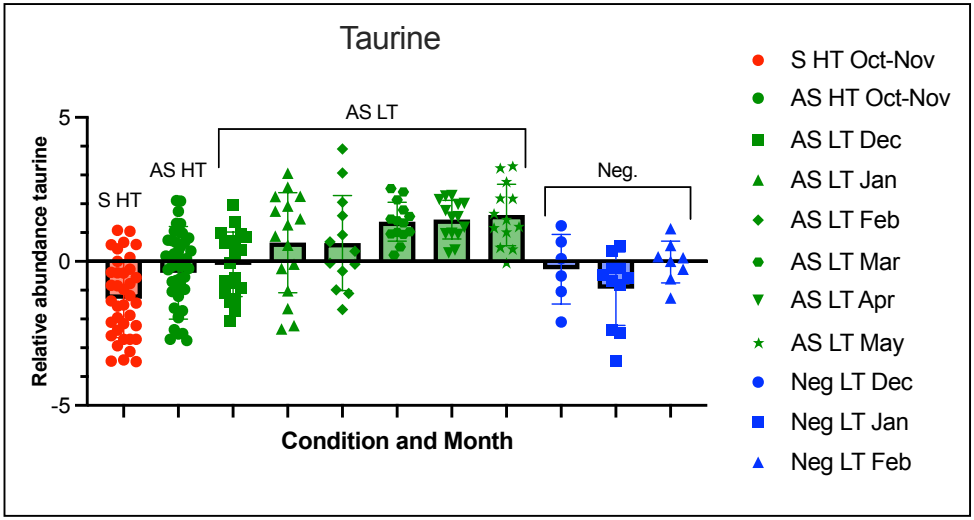

Figure S3

A

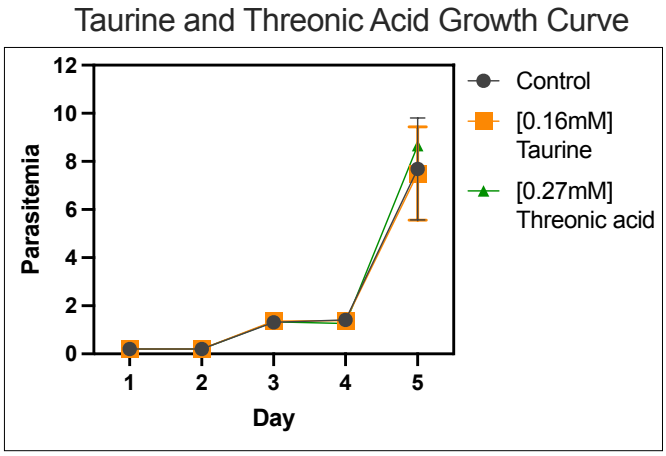

C

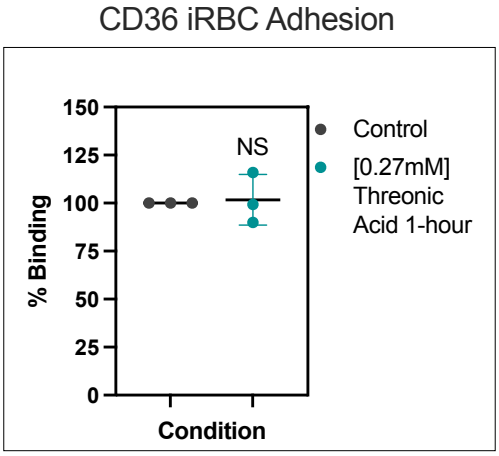

B

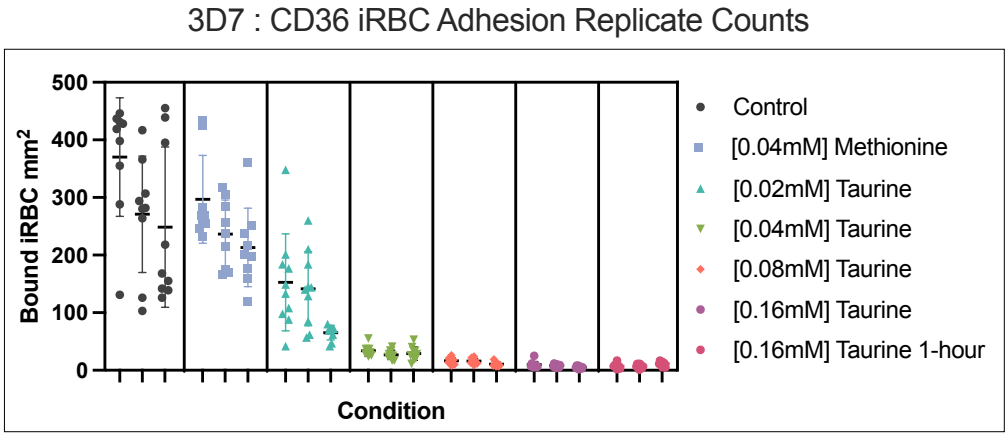

D

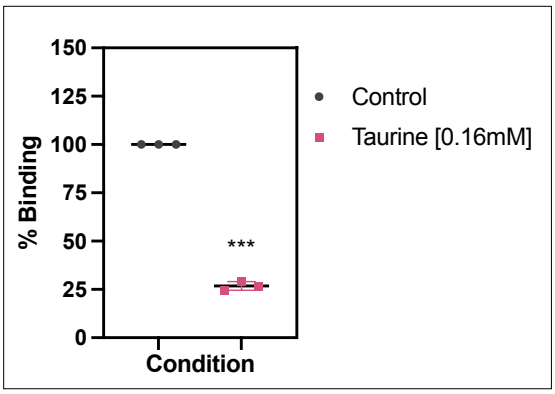

E

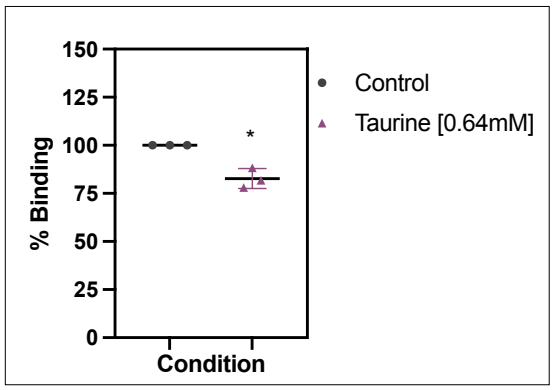

F

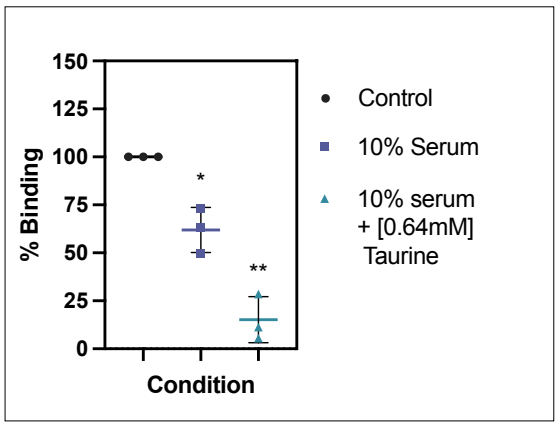

Figure S4

A

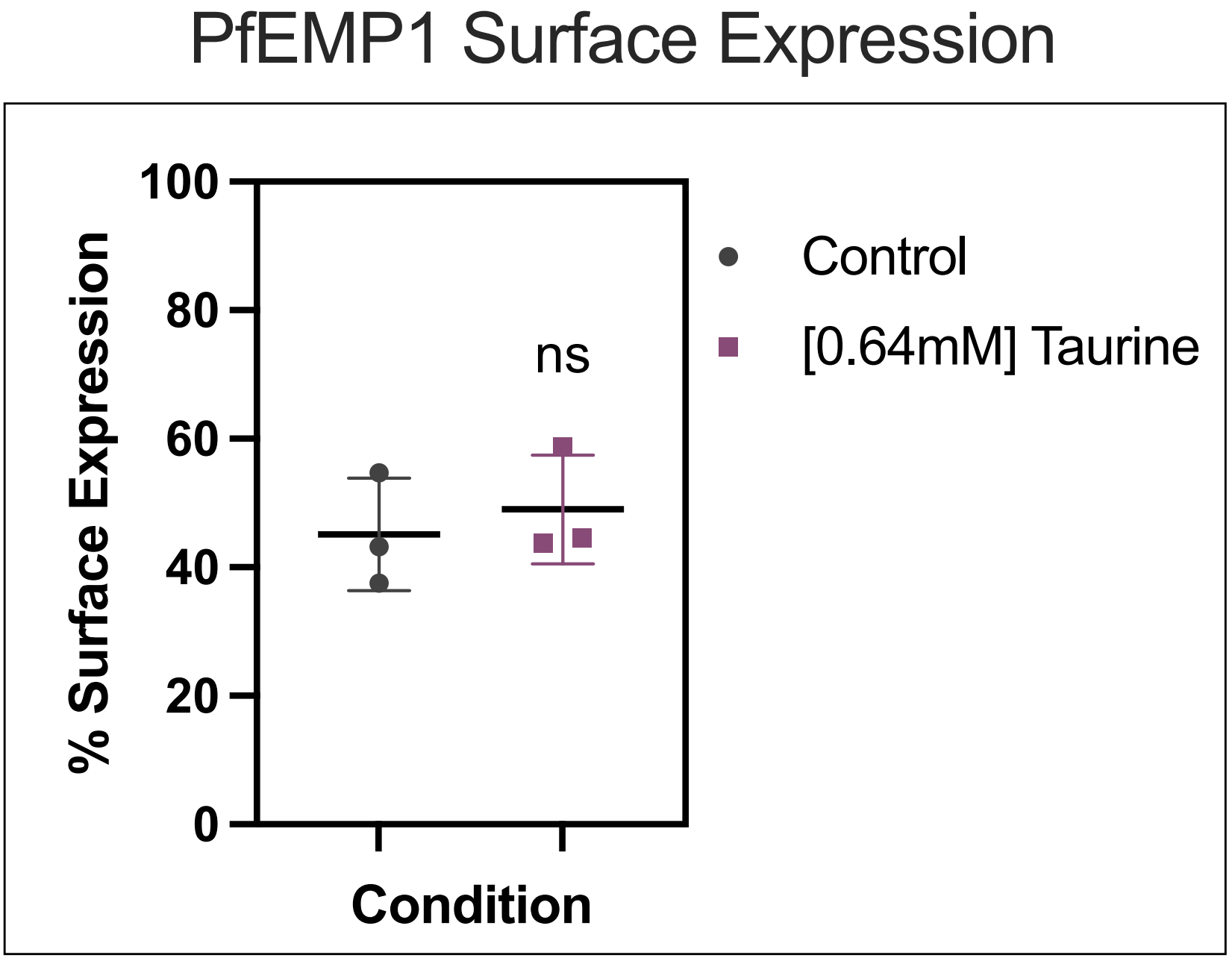
PfEMP1 Surface Expression
100
80
60
40
20
0
% Surface Expression
ns
Condition
Control
[0.64mM] Taurine

Figure S4

B

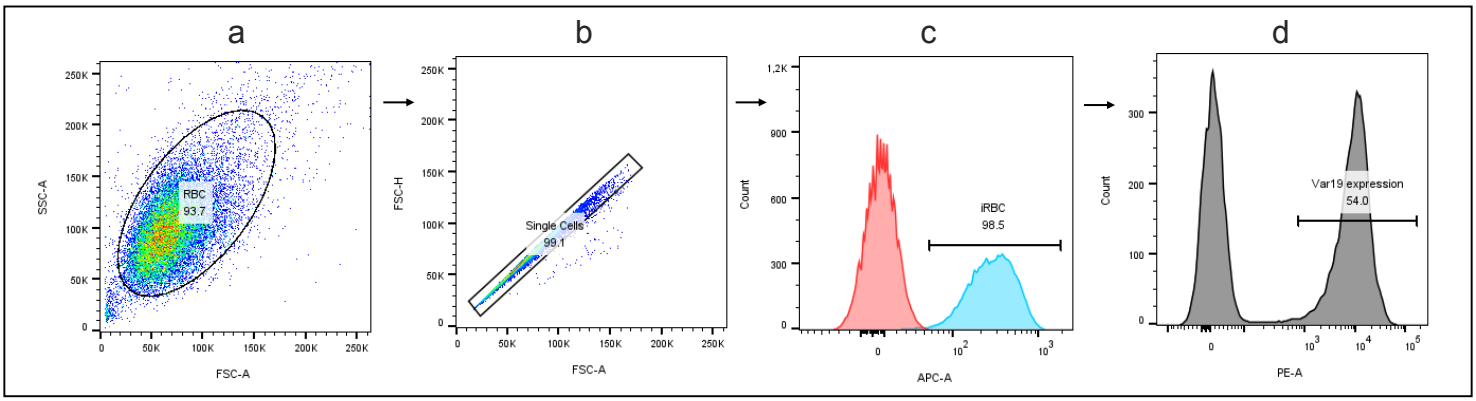

C

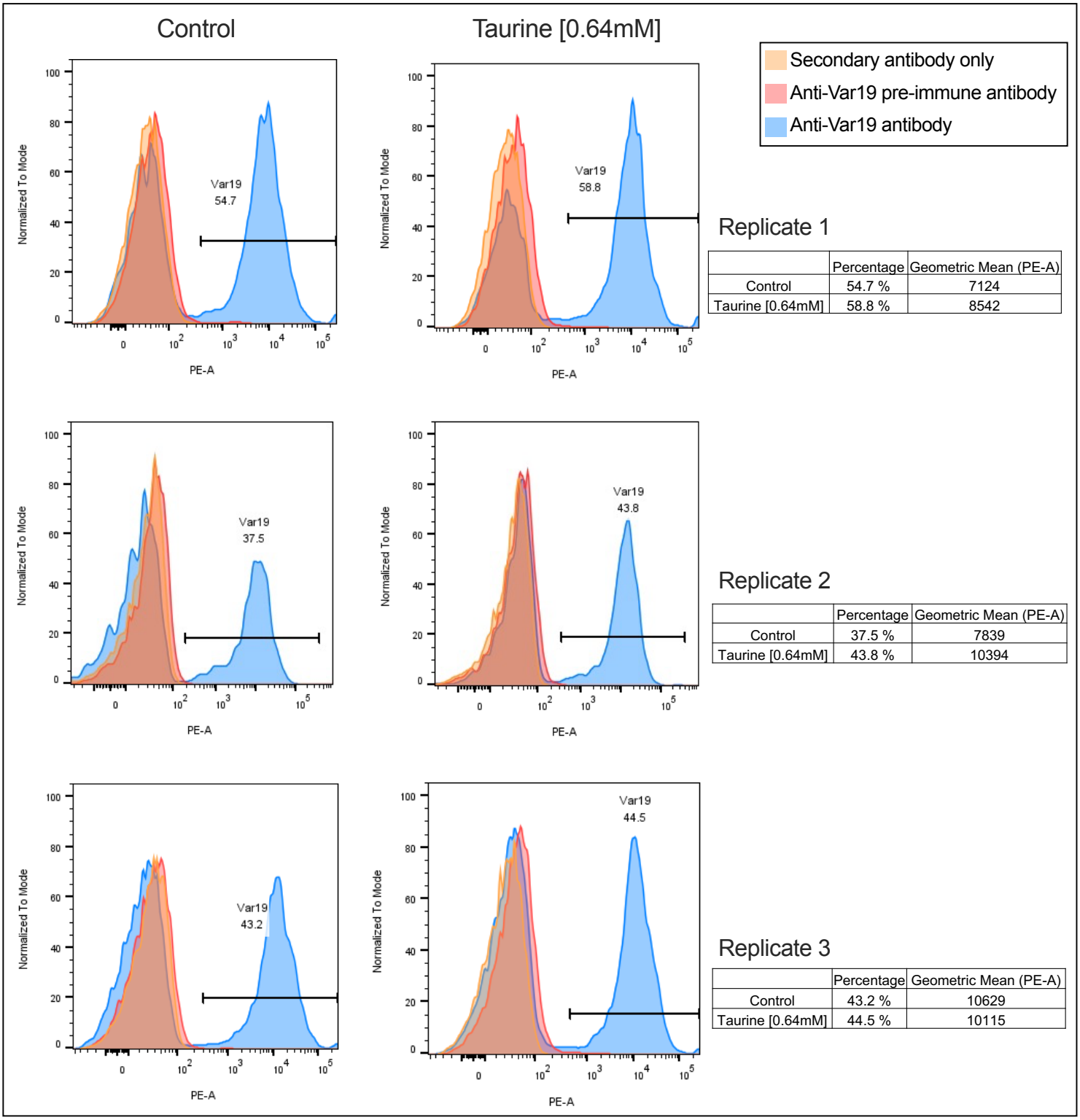

Replicate 1

	Percentage	Geometric Mean (PE-A)
Control	54.7 %	7124
Taurine [0.64mM]	58.8 %	8542

Replicate 2

	Percentage	Geometric Mean (PE-A)
Control	37.5 %	7839
Taurine [0.64mM]	43.8 %	10394

Replicate 3

	Percentage	Geometric Mean (PE-A)
Control	43.2 %	10629
Taurine [0.64mM]	44.5 %	10115

Figure S4

D

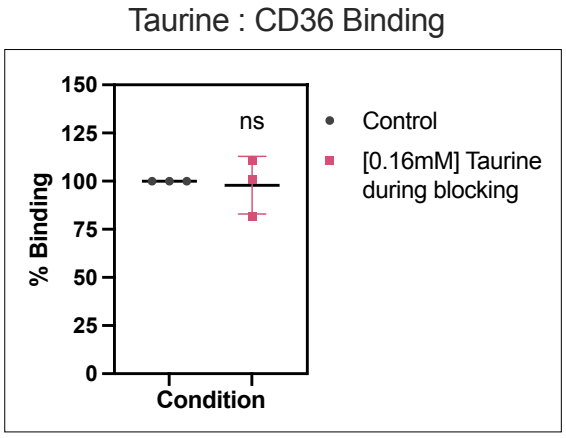

E

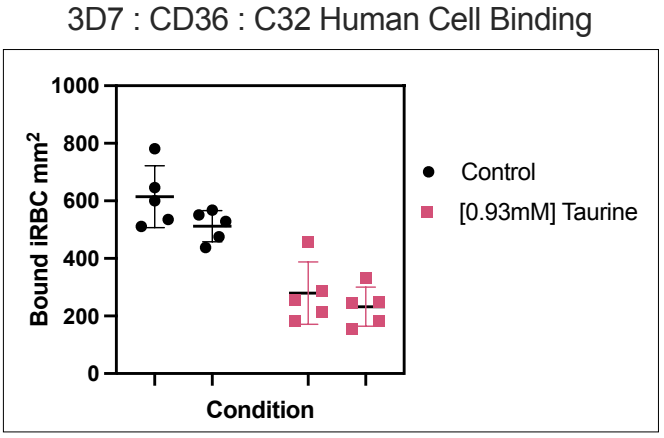
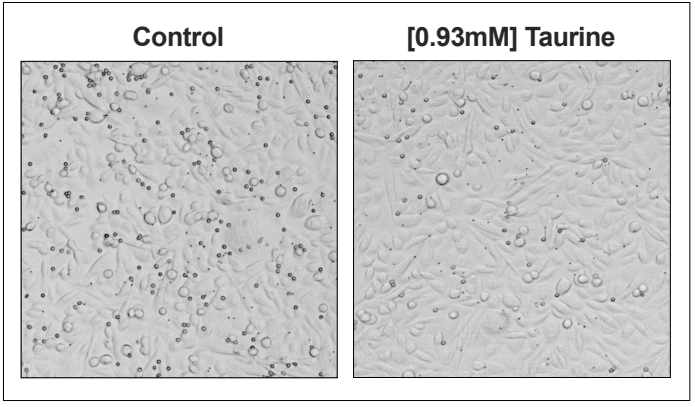
F